Digitalized Earth's most severe sea-level regression and extinction

Mingxing Dong (dongmingxing@hgu.edu.cn)
Hebei GEO University

Research Article

Keywords: extinction, sea-levels,

Posted Date: April 13th, 2021

DOI: https://doi.org/10.21203/rs.3.rs-400115/v1

Review version

Digitalized Earth's most severe sea-level regression and extinction

Ming-Xing Dong

Earth Sciences Academy, *Hebei GEO University, Shijiazhuang 050031, China*

Corresponding author: dongmingxing@hgu.edu.cn
Phone:13073102906

Submitted to *Scientific Report* (2021)

Abstract: ~ 212 words

Text: ~ 6066 words

Figures: 9

Tables: 2

Abstract

End-Permian mass extinction is the largest bio-crises in the past 542 million years in Earth's history. Despite half a century of study, what caused the catastrophe remains equivocal. Fossil collections in the study area of Bayan Har, NW China, suggest a continuous Permian sequence, whereas most mid-to-upper Permian strata were missing. By correlating the Permian sequence reconstructed from reworked carbonate clasts with the measured Permian section, we corroborate a sea-level fall of at least 354 m caused by plume-induced uplift, resulted in the erosion of the last 15-Myr Permian carbonate strata, from Uppermost Permian to the fusulinid zone. The marine regression and resultant erosion occurred not only in China but also in Canadian Arctica[1], Oman[2], Canadian Rockies[3], Norway[3], North America[3] all over the world. New sections and digitalized sea-level regression demonstrate that the period of extinction falls within the hiatus, a break in deposition between the uppermost Permian carbonate strata and the clasts reworked from Permian platforms, representing a duration of sea-level drop 354 m. Carbonate clasts, Siberian Traps volcanism, global warming, anoxia, and ocean acidification are all post-extinction geological events. Why did the extinction occur during the falling stage? We will never know because we can't study a hiatus unrepresented by strata unless we associate the extinction with the sea-level drop.

1. Earth's most severe sea-level regression neglected

End-Permian Mass Extinction (EPME) is the most severe biodiversity crash in the past 542 million years. Despite half a century has passed, what caused the catastrophe remains unexplained. Geological events, e.g., global warming[4-8], negative excursions of $\delta^{13}C$ and $\delta^{18}O$, Siberian Traps volcanism[8-10], anoxia[6, 11], ocean acidification[10, 12], etc. are proposed mechanisms to interpret EPME. However, these events based on the transgression records produced in isolated or semi-isolated basins from the Panthalassa postdated EPME. These authors failed to recognize a severe regression represented by a hiatus across the Permian Triassic Boundary (PTB) interval.

The PTB sections in Meishan[13, 14], Penglaitan[9], Qiangtang[15], Nanpanjiang[16], South China, Armenia, and Iran[8] are marine incomplete. The strata contain exclusively organic-rich rocks or bear euryhaline organisms (e.g., gastropods, ostracods, or claraia, etc.), which reflected a terrestrial input of fresh water and plant matter resulting in the observed $\delta^{18}O$ lower or a reconstructed temperature higher than predicted.

Of all the basins mentioned above, the Meishan basin was the deepest and minimally affected by the regression, and the observed $\delta^{18}O$ values are the highest, or the reconstructed temperatures lowest. The deeper the basin, the lower the sediment accumulations are, and the thinner the extinction bed. Only under a condition of precipitation＞evaporation could a sequence maintain growth or be represented by a hiatus or a condensed bed. Therefore, the ocean record of lower $\delta^{18}O$ is potentially preserved in marine sediments, whereas the higher $\delta^{18}O$ or the reconstructed lower temperature record was missing when ocean basins were isolated or semi-isolated from the Panthalassa. The deeper water depth is responsible for, the lower temperatures reconstructed in the Meishan basin, which was minimally affected by the global regression rather than by the rapid evaporation[8], whereas the shallower water depth is responsible for, the higher temperatures reconstructed in Armenia and Iran sections[8], which was maximally affected by the global regression. Penglaitan[9] was nearer the equator and could have more considerable evaporation than Meishan, whereas its constructed temperatures aren't lower than Meishan, suggesting that the $\delta^{18}O$ index wasn't available in shallow-water shelf areas, which was maximally affected by the sea-level drop of 354 m. The PTB sections in Armenia and Iran may have contained a more extensive hiatus because a

vertical fall of 354 m in global sea level translates into 35400 m of horizontal loss on a flat coast or marsh.

2. Digitalized geological events across the PTB interval [Fig.1]

Analysis of the cause(s) of EPME in the last 20 years has widely applied high-precision U-Pb geochronology and conodont biostratigraphy. The extinction event is recorded on 251.939 ± 0.031Ma[9]. The time-equivalent regression in whole South China is constrained to *Clarkina meishanensis* and *Hindeodus changhsingensis* zones, staying for ~50-100 ka[17], which is consistent with global regression hiatus "***a duration of 89 ± 38 kyr for the Permian hiatus and of 14 ± 57 kyr for the overlying Triassic***" [18]. In other words, the last 89-kyr Permian strata had been eroded in South China during the first 14-kyr Triassic regression.

The absolute ages of geological events are an unwarranted certainty, but the relative ages based on superposition are certain. In the North Changma River section, more pebbles and boulders are reworked from Middle Permian than from the Upper one, suggesting a longer time for the low-stand duration than for the sea-level drop and rise. We set the end Permian at 251.939 Ma[9] and divide the first 14-kyr Triassic regression interval into three parts: ~3 kyr for the sea-level fall, ~8 kyr low-stand lasting, and ~3 kyr for rising to the previous level. Geological events would occur in chronological order and spans as follows:

2.1 The period of extinction falls between 251.939 and 251.936 Ma

According to the sections of North Changma River and Xiadawu [Fig.2D], there is a hiatus [Fig. 1, Fig. 2D, a] between the uppermost Permian strata and the overlying conglomerates. If no uppermost carbonate strata were missing, EPME would have occurred at 251.939 Ma[9]. If some eroded, EPME would have fallen within the 3-kyr-long hiatus, a break in deposition represented the duration of the sea-level drop from the uppermost Permian to the middle Permian fusulinid zone, separating the Changhsingian shales from the overlying Triassic conglomerates [Fig.2D]. The Permian-type species can't survive a hiatus, and the conglomerates reworked from Permian platforms are post-extinction events.

With the lowering of sea level, the extinction rates are greatly enhanced [19-21]. The basins fully-connected with the Panthalassa shared the same extinction period, whereas the isolated or semi-isolated basins shared a different extinction time, as indicated by [13][Fig. 3], depending upon the relative input rates of freshwater and plant matter and the salinity diluted states.

Less than 1 centimeter in thickness of the hiatus-equivalent bed is inferred from the general sediment accumulation rates of 0.36-0.17cm/ka [14]. It would not be available to find out a complete PTB sequence[22] with higher resolution. All the PTB sections are represented either by a centimeter-thick extinction bed in distal basin center areas or by a hiatus in a shallow-water shelf environment.

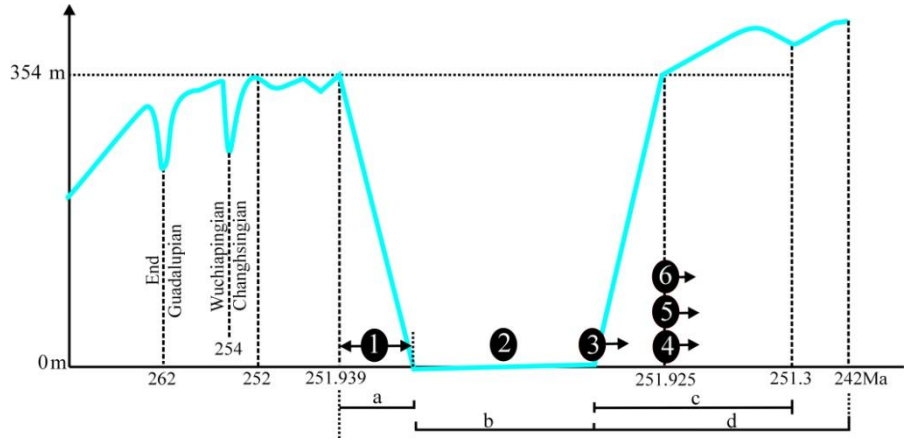

Fig.1 Digitalized geological events (numbered black circles) and the corresponding relative magnitude (green curve) across the PTB interval: (1) extinction event, (2) minimum values of $\delta^{13}C$, (3) initiation of Siberian Traps volcanism, (4-6) onset of warming, anoxia, and ocean acidification, etc.; Numbered lines (a to d) represent a ~3 kyr-long period for sea-level drop (extinction hiatus), ~8 kyr sea-level low-stand, sea-level rise ~0.6 Myr, and volcano eruptions ~10 Myr, respectively.

2.2 The minimum $\delta^{13}C$ record at 251.932 Ma

A systematic decreasing trend in $\delta^{13}C$ value is suggested[23] from basin margin to basin center or from stratigraphic position to EPME both below and above. Sediments in the distal basin center areas preserved the minimum $\delta^{13}C$ values, where few Permian records were missing. The minimum $\delta^{13}C$ values were maintained at a depth of ＞354 m, during marine regression interval between 251.939 and 251.925 Ma, with the lowest sea-level occurring at 251.932Ma. The negative excursion of $\delta^{13}C$ isn't considered related to EPME due to reduced carbon-isotope shifts with decreasing stratigraphic distances to EPME[23].

Because the average $\delta^{13}C$ values of CO_2 released suggest a source of large quantities of carbonate-derived carbon[10], removing at least 354 m-thick carbonate rocks during the end Permian regression period best explained the negative excursion of $\delta^{13}C$. A delayed source with small quantities of carbon from sill intrusions[24] or thermal erosion[25] showing a homogenized $\delta^{13}C$ trend[26] failed to explain the globally recognized excursion of $\delta^{13}C$[27]. A negative shift in $\delta^{13}C$ occurred before the onset of volcanism, global warming, or negative

excursion of $\delta^{18}O$ has been verified[8].

2.3 Initiation of volcanism at 251.928 Ma

Volcano eruptions occurred at the end of the low-stand interval at 251.928 Ma, as indicated by the Xiadawu section[Fig. 2D][28], containing a 752-m-thick volcano with two complete breccia-tuff-basalt cycles, which witnessed an uplift-erosion-basalt process, following the rule of Campbell's plume theory[29]. Volcano eruptions would lead to subsidence of basaltic ocean bottom and sea-level rise.

2.4 Global warming and anoxia events at 251.925 Ma

Global warming and anoxia events didn't occur with the volcanic event synchronously until sea level rise to the previous level at 251.925 Ma, due to the low-stand interval corresponding to a cooling event[18], as indicated by a *Clarkina* specimen showing a higher $\delta^{18}O$ value of 19‰[9]. The Xiadawu Volcano with an upper age limit of 247.2 Ma from overlying fossils[28] and a lower age limit at 254±2 Ma from a 3-meter-thick tuff bed[30] indicates the synchrony with Siberian Traps volcanism. Their eruptions coincided with the onset of early Triassic major transgression.

Above geological events based on the incomplete PTB sections occurred very close to the extinction event but never preceded it. A fluctuation of temperature ~3-7°C [8, 9, 16] is not severe enough to cause the largest bio-crises. Moreover, the regression-induced conglomerates are consolidated by calcareous (85%) and ferric (15%) oxides, suggesting an un-happening of ocean acidification or anoxia during the extinction interval. All of the above direct towards that a regression-extinction mechanism might be an un-neglected reasonable cause.

3. Interpretation for EPME occurred during the falling period

Last century, Newell N. D. proposed the regression-extinction relation[19]. He ascribed the extinction to the reduced habitat regions, which significantly enhanced the competition and predation. Schopf[20] estimated a sea-level drop of several hundred meters due to "***water withdrawing into a deepening ocean basin***," linking it to "***sea-floor spreading***." Hallam proposed "***the case for sea-level change as a dominant causal factor in mass extinction of marine invertebrates***." [21]

Failing to comprehend the magnitude, timing, and duration of the End-Permian regression,

Hallam[3] didn't think Newell's theory tenable for interpreting EPME. But he provides a series of crucial evidence supporting the end-Permian regression. "***all sections, the latest Permian is missing, and lower Triassic strata rest unconformably on middle Permian or older strata…… the oldest Triassic rocks has been lacking.***" Correlation between these sections in North America, Norway, and Canadian Rockies[3] and those in Canadian Arctica[1], Oman[2], and Chinese Bayan Har are perfect, where the last 15-Myr Permian carbonate strata were missing during the oldest Triassic times. The same global event (End-Permian regression) occurred in different places (e.g., North America, Canadian Rockies, Chinese Bayan Har Basin), but different authors[3, 31, 32] interpreted it in an identical wrong way [Fig. 2B]: "***conodonts ……have shown that so-called basal Triassic strata are in fact of Changhsingian age***" [3, 32]. Both involved reworking and redeposition during the falling period, the carbonate platforms bearing the latest Permian ammonoid markers, and the deep-slope shales containing the Changhsingian Age [Figure 2].

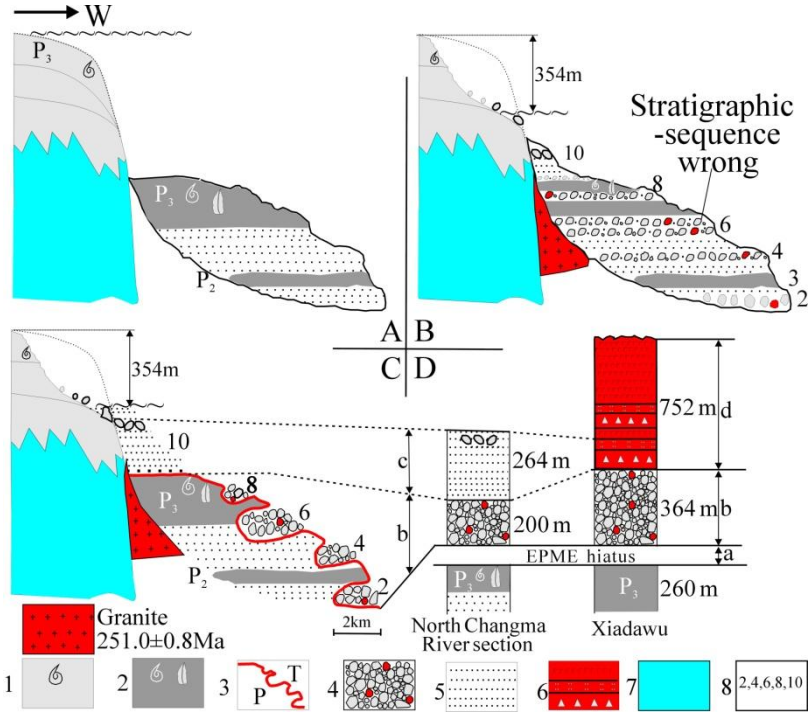

Figure 2. In the North Changma River section, End-Permian faces of shallow-marine and deep-slope are showing before (A) and after (B, C, D) marine regression, as well as a correlation of the PTB sections (D) between North Changma River (left) and Xiadawu (right). Numbered lines (a to d) represent a period for sea-level drop (extinction hiatus), sea-level low-stand, and sea-level rise, as well as volcanic eruptions, respectively, as shown in Fig.1. Legends: (1) Latest Permian limestone ammonoid, (2) Shale bearing Changhsingian conodonts, (3) P/T boundary, (4) Conglomerates, (5) Sandstone, (6) A volcano cycle of breccias-tuff-basalt, (7) Carboniferous-Permian sequences, (8) Bed No. in North Changma River section.

The reworked bioclastic conglomerates should overlie the shale bed bearing Changhsingian

conodonts [Fig.2C], rather than be overlain by it [Fig.2B]. When turbidity currents activated erosion and transportation of conglomerates, which had excavated into the unconsolidated marine shales, it also resulted in the shales' reworking. One may have failed to recognize a hiatus or a regression sequence (sandy conglomerates) between the black shales bearing Changhsingian conodonts and the overlying Triassic units. Hallam's ***"widespread absence of latest Permian ammonoid markers……coincides with a major transgression***"[3] neglected the earliest Triassic regression or hiatus, which occurred between the transgression intervals of the latest Permian and the Early Triassic. The ammonoid markers didn't happen in a regression sequence of the earliest Triassic Age due to its centimeter-thick condensed bed or hiatus. Hallam proposed critical evidence supporting the end-Permian regression that the conglomerates bearing the latest Permian ammonoid markers rest on Changhsingian conodonts. In Salt Range sections, ***"rather abraded nature of the bioclasts, brachiopods and foraminifera range up to the upper part of the Kathwai Dolomite, which is of late Griesbachian age, and then go extinct"*** [33]. All reworked carbonate breccias, including the "***rather abraded nature of the bioclasts*****,"** are attributed to the end Permian regression of sea level, although some occurred in early Griesbachian deposits, others in middle or late ones. The easily-transported boulders or pebbles occurred in early Griebaschian deposits, whereas those difficult-delivered breccias deposited in situ occurred in later sediments. Carbonate breccias appeared in Bed 11 (66.35m, late Griesbachian Age) of the West Changma River section, bearing the uppermost Permian fossils. Some abraded boulders or pebbles occurred in Beds 2-8 (early-to-middle Griesbachian Age) and Bed 12 (late Griesbachian Age) of the North Changma River section, containing the mid-Permian fusulinids. The carbonate bioclasts reworked from the underlying Permian platform are embedded by "***the upper part of the Kathwai Dolomite, which is of late Griesbachian age*****"** in the aftermath of redeposition. A sharp increase in Sr^{87}/Sr^{86}[34] is consistent with the intensified weathering[5, 35], enhanced terrestrial input, and anomalous marine sediment fluxes[36, 37], which promoted sediment loading, resulting in sediment redeposition.

Although the global regression duration is timed at the decamillennial timescale[17, 18], calibrating its magnitude has never been done. This paper deals with the extent of marine regression in the Bayan Har basin, NW China that has received various debates. Here, we

corroborate a global sea-level fall of 354 m during the end of Permian by compiling the published fossil collections [Fig.3] and correlating the Permian sequence reconstructed from reworked carbonate clasts with the measured Zhihela section.

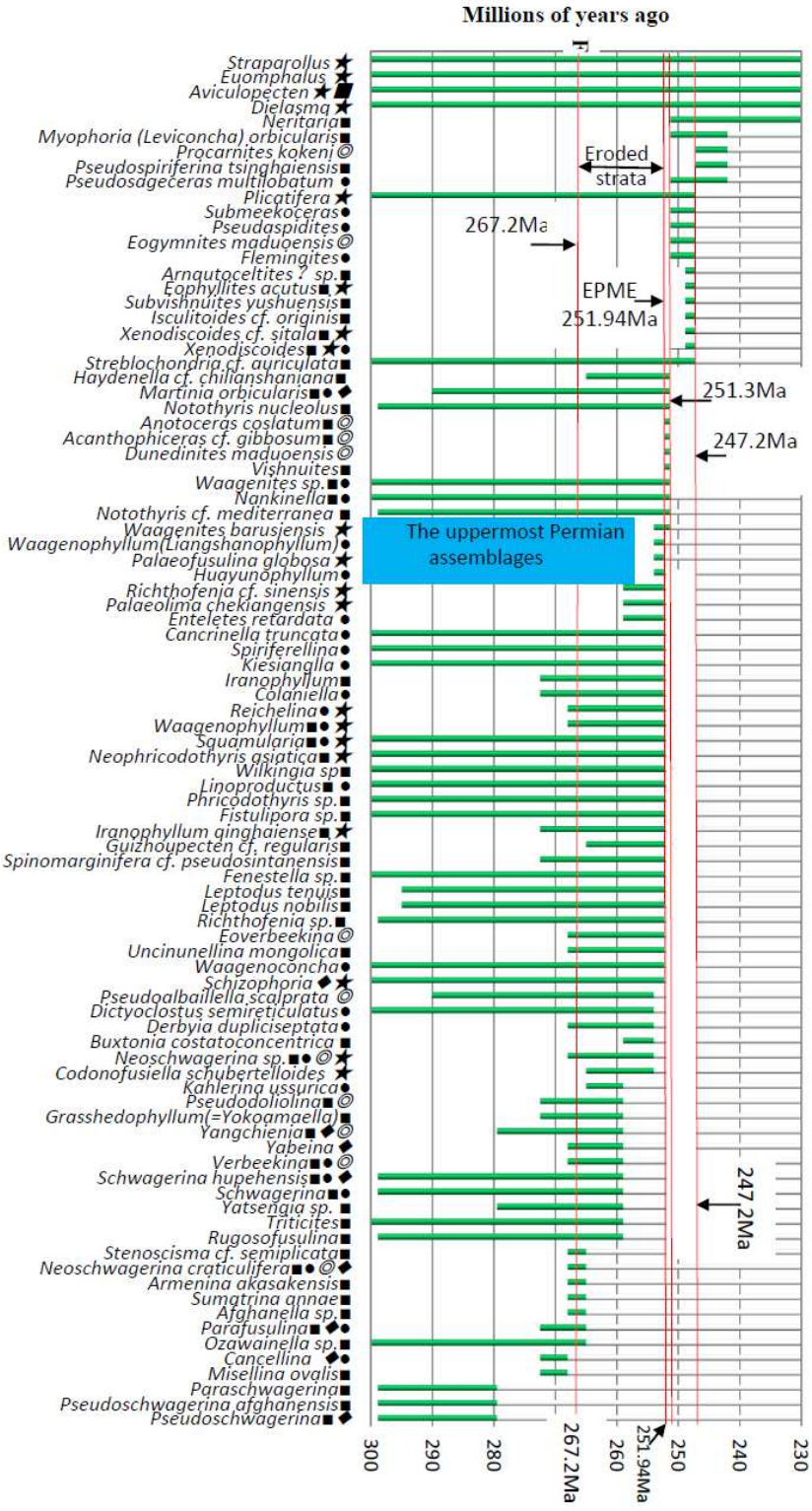

Figure 3. Time-series biostratigraphy across the PTB (~251.94 Ma) interval in the study area; Green-bar is showing the lifespan of the organisms sampled in the studied area based on the database of fossil websites (fossilworks.org); Solid arrows and red lines are dated horizons. The sampling area showing ●Huashixia (the south

slope of East Kunlun[38-40], Donggeicuona Lake[41], Long-Rock Mountains[41]); ■Changma River[31, 42] (Youyun, Yama); ◎Maduo (Zaling lake paleo-seamounts[38], 24 km eastern Maduo[42, 43]); ★Shixia[44, 45] (Maqin town, Zhihela[31], Aliza[31]). A sea-level drop of 354 m results in as thick as 533-m strata were eroded from the uppermost Permian to the basal fusulinid zone, between the two red lines 251.94 Ma and 267.2 Ma. The blue rectangle shows the index fossils of the topmost Permian.

4. Geological setting and sections

The subsidence of the Bayan Har ocean was initiated during the Late-Paleozoic Time by rift[46]. Continued passive subsidence resulted in a very thick and continuous deposition until the late Triassic orogenic activity, which ended the basin deposition. Bayan Har basin is now an area of ＞700,000 km^2[46] with 2300 km long, 200- to 1000-km wide, and 14-km thick Triassic slate-dominated siltstone depocentre [Fig.4].

An erosional unconformity represents a majority of PTB sections [Fig.4B], e.g., North Changma River[31], Mentang[47], Bocigou[48], Rilagou[49], and Yalong River[42], along the passive continental margin of Bayan Har basin separating the lower Permian from the overlying lower Triassic. Carbonate conglomerates, giant blocks, or kilometer-sized megabreccias reworked from the Permian platforms. They occurred in slope turbidites or the latest Permian siliceous mudstones in distal basin center areas. Or enclosed by early Triassic radiolarian cherts/shales in basin center areas [Fig.4B], e.g., Eling Lake[38]; two sides of the Ganzi-Litang fault zone; eastern & western mélange zones of Jinsha River[46]; Bailong River and Xihanshui Basins; and Liufengguan Town, Fengxian, etc..

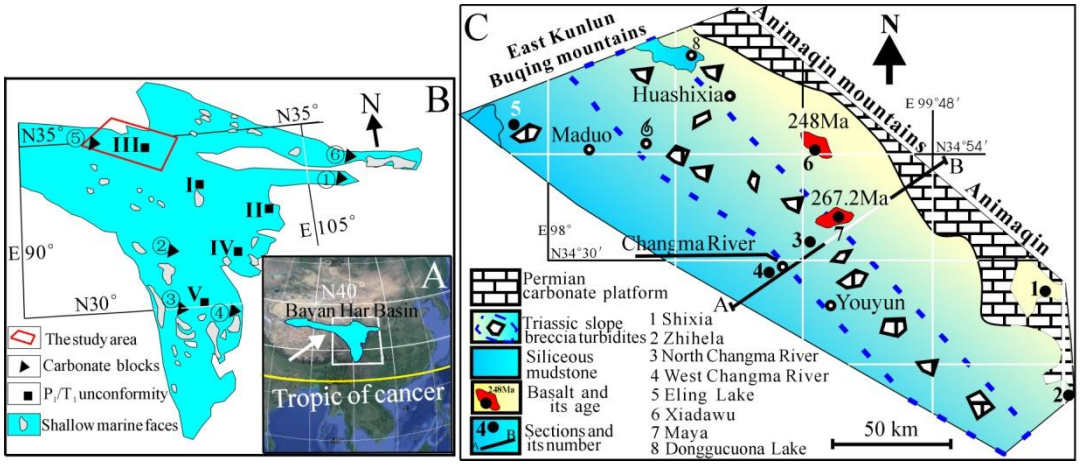

Figure 4. (A) The outline of Bayan Har basin in West China; (B) Paleogeography during the PTB of the Bayan Har Ocean: the red rectangle showing the study area, numbered squares (I to V) are localities representing an erosional unconformity separating Early Permian from the overlying Early Triassic: (I) Mentang[47], (II) Bocigou[48], (III) Changma River[31], (IV) Rilagou[49], (V) Yalong River[42], and numbered triangles (① to ⑥) [38, 46] are reworked carbonate clasts distributing in ①Lueyang, ②Jinsha River, ③Litang, ④Ganzi, ⑤Eling Lake, ⑥Fengxian; and (C) Late Permian to Early Triassic paleogeographic map of the study area: numbered circles (1 to

7) showing the locations of studied sections (1) Shixia, (2) Zhihela in the carbonate platform in the east, and lower-slope (3) North Changma River and (4) West Changma River of early Triassic turbidites in the southwest circled by dashed line enclosing carbonate collapse, (5) Eling Lake in the center basin areas, volcanos of (6) Xiadawu and (7) Yama in the middle study area.

The study area [Figure 3C] is located at the northeastern margin, extending along the south edge of the Buqing Mountains in the southeast through Huashixia, Youyun, and Zhihela over an area of 15,000 km^2. The Permian shallow-water carbonate platform distributed in the east, and the marine siliceous mudstone distributed in the west. The continent-ocean transition is the overlying first Triassic turbidites (Changma River Formation). The upper Permian (Gequ Formation) shallow-water faces are rarely preserved, with relict outcrops occurring in Gequ and Zhihela, southeast of the study area. In contrast, middle Permian (Maerzheng Formation) limestones intercalated with basalts are well preserved. The number and extension of Permian carbonate outcrops decrease markedly toward SWW due to increasing Permian erosion and the Triassic cover of slates intercalated with siltstones.

Roughly on the AB profile [Figure 4C], from the eastern carbonate platform in Gequ to the western deep-sea megabreccias in Eling Lake, a series of sections [Figure 5] are introduced as follows:

4.1 Gequ section in Shixia[43, 44] (100°17′E，34°23′N), Maqin county

The upper part of this section (Gequ Formation) contains 300-m-thick bioclastic limestones, with an End-Permian extinction horizon on the top of Bed 7 (50 m) bearing a *Palaeofusulina-Reichelinia-collaniella* assemblage, which can correlate with Beds 1-2 immediately underlying the PTB in Chongyang section[50].

4.2 Zhihela section (34°3′37.97″N, 100°22′7.54″E)[31] Page34

The section [Figure 5] is located in a near-rectangular residue with about 15 square kilometers on a ridge north of Zhihela, Gande, representing an almost complete Permian and Lower Triassic sequence. The middle Permian bioclastic rudstone Bed 2 (63.69 m) is conformable with the underlying lower Permian thin-bedded fine quartz sandstone. Bed 3 (52.11 m) comprises purplish-red thin-bedded wackestone. Bed 4 (63.81 m), gray-purple bioclastic limestone, bears *Neoschwagerina* sp. and *Pseudofusulina* sp.; Bed 5 (39.13 m) purplish-red gravel-sized rudstones; Bed 6 (12.32 m), gray massive bioclastic rudstones; Bed 7 (53.44 m), purple-red mudstone slates with lesser amounts of pebbly sandstones; **the**

regression Bed 8 (192.3m), purplish-red intraclasts rudstones showing a sedimentary structure of storm deposits; **the uppermost Permian Bed 9** (56.52 m), gray bioclastic limestone yields *Neophricodothyris* sp. and *Iranophyllum* sp. **The earliest Triassic regression Bed 10** (98.6 m), purplish-red intraclasts rudstones; Bed 11 (816.97 m), massive grey limestone bearing gastropod *Straparollus* sp. and *Euomphalus* sp.; Beds 12-15 (97.56 m), purplish red, grey impure rudstone contains gravel- to sand-sized intraclasts carbonate particles; Bed 16 (120.76 m), feldspar sandstone. 20 m below Bed 2 of the Zhihela section is a 20-m-thick basalt lenticular body. The impingement of basalts on the base of the fusulinid zone[38] suggests a later basalt.

4.3 North Changma River section[31] (Figure 46 p64, p65 Figure 47) (34°32.68′N, 99°12.9′ E)

This section (Changma River Formation) [Figure 2C, 2D; Fig.5; Fig.9] formed a deep slope setting, containing a regression part and an overlying transgression one. Wave-formed ripple marks and beddings indicate its ascending order. The regression part (Beds 2-9) includes four lenses of conglomerates (a lens with 2km long, tens of meters high) with a total of 200-m thick, which were reworked from shallow-water platforms and embedded in a matrix of slates (50m), silt-slates, siltstones or sandstones (431m) of deep-slope faces. Sandy conglomerates are composed of limestone (65%), basalt (25%), sandstone (5%), and slate (5%), well-rounded, but poorly sorted, centimeter to meter-sized boulders and pebbles, cemented by calcareous (85%) and ferric (15%) oxides. The clastic-supported wave-polished sandy conglomerates, numerous 10-m-sized collapse, several 100-m-sized giant breccias, and some kilometers-sized blocks all reworked from the last 15-Myr Permian platforms, bearing assemblages of foraminifers, calcareous green and red algae, rugose corals, brachiopods, calcareous sponges, and bivalves.

The transgression part (Beds 10-12) includes Bed10 (264 m) with thin-medium feldspar-quartz sandstones and occasional silt-slates; Bed 11 (90 m) silt-slates interbedded with fine-medium sandstones; Bed 12 (874m) with thinner beds of fine-medium greywackes intercalating with occasional occurring of slates. The greywackes contain 10- to 40 cm-sized limestone breccias of reworked Permian fauna, including *Aviculopecten* cf. *kunlunensis*, *Neophricodothyris* (*Phricodothyris*) *asiatica*, *Waagenophyllum* sp. and *Neoschwagerina*.

Bed 11 contains post-extinction organisms widely distributed in Changma River[31, 42] and

312 24km east of Maduo county[45, 51]. The joint occurrence of the Last Appearance Datums
313 (LADs) (252.3-251.3Ma) (http://fossilworks.org/) of *Vishnuites* sp., *Dunedinites maduoensis*,
314 *Acanthophiceras* cf. *gibbosum*, *Anotoceras coslatum* and the First Appearance Datums (FADs)
315 (251.3-247.2Ma) of *Neritaria* sp., *Eogymnites maduoensis*, *Eophyllites crassus*, *Dieneroceras*
316 sp., *Cordillerites* sp., and *Arnautoceltites* sp. narrows the age estimate for Bed 11 at 251.3 Ma.

317 **4.4 West Changma River section(34°28′N, 99°9′30″E)** [28]page69 [43]Page241

318 In ascending order from east to west, the section contains lower-slope faces of silty
319 slate-dominated turbidites representing Early-Triassic deposits over 3000 m. Taupe
320 medium-thin Bed 1 (＞62.13 m) comprises mid-fine grained sandstone with silty slates;
321 interbedding of light grayish-green medium-thin Bed 2 (336.80 m) and feldspar greywacke
322 and silty slates; medium thin Bed 3 (393.37 m) bearing medium-fine-grained feldspar quartz
323 sandstones intercalated with silty slates; Taupe low-metamorphic Bed 4 (244.08 m)
324 medium-coarse-grained feldspar sandstones intercalated with a minor amount of silty slates;
325 light grayish-green low-metamorphic Bed 5 (74.83 m), muddy fine-grained feldspar quartz
326 sandstones intercalated with silty slates; Grayish and white Bed 6 (14.16 m), massive
327 limestone; Grey Bed 7 (165.86 m), fine-grained silty slates intercalated with medium-thin
328 bedding medium-fine grained feldspar sandstones, and with occasional occurring of limestone
329 lenses bearing early Spathian ammonites *Isculitoides* sp. and *Arnautoceltites* sp.; Taupe low
330 metamorphic medium-thin Bed 8 (63.82 m) medium-fine-grained feldspar quartz sandstones
331 intercalated with silty slates; Grey medium Bed 9 (2.79 m) bio-clastic limestones bearing late
332 Spathian ammonites *Isculitoides* cf. *originis*, *Isculitoides* sp., *Subvishnuites yushuensis*, and
333 *Eophyllites acutus*. Taupe, low metamorphic medium-thin Bed 10 (549.08 m) comprises
334 muddy fine-grained feldspar quartz sandstones intercalated with silty slates, showing
335 oscillating ripple marks. **Carbonate brecciated 11 (66.35 m) bears Permian *Iranophyllum***
336 **sp., *Neophricodothyris* cf. *asiatica*, and *Wilkingia* sp. assemblages, persisting to the**
337 **extinction zone**. Taupe, low metamorphic, medium-thin Bed 12 (98.15 m),
338 medium-fine-grained feldspar quartz sandstones intercalated with silty slates. Beds 13-19
339 (1131.39 m), Gray silty slate with grayish-brown medium-fine feldspar quartz sandstone
340 containing hundreds of meters of carbonate boulders.

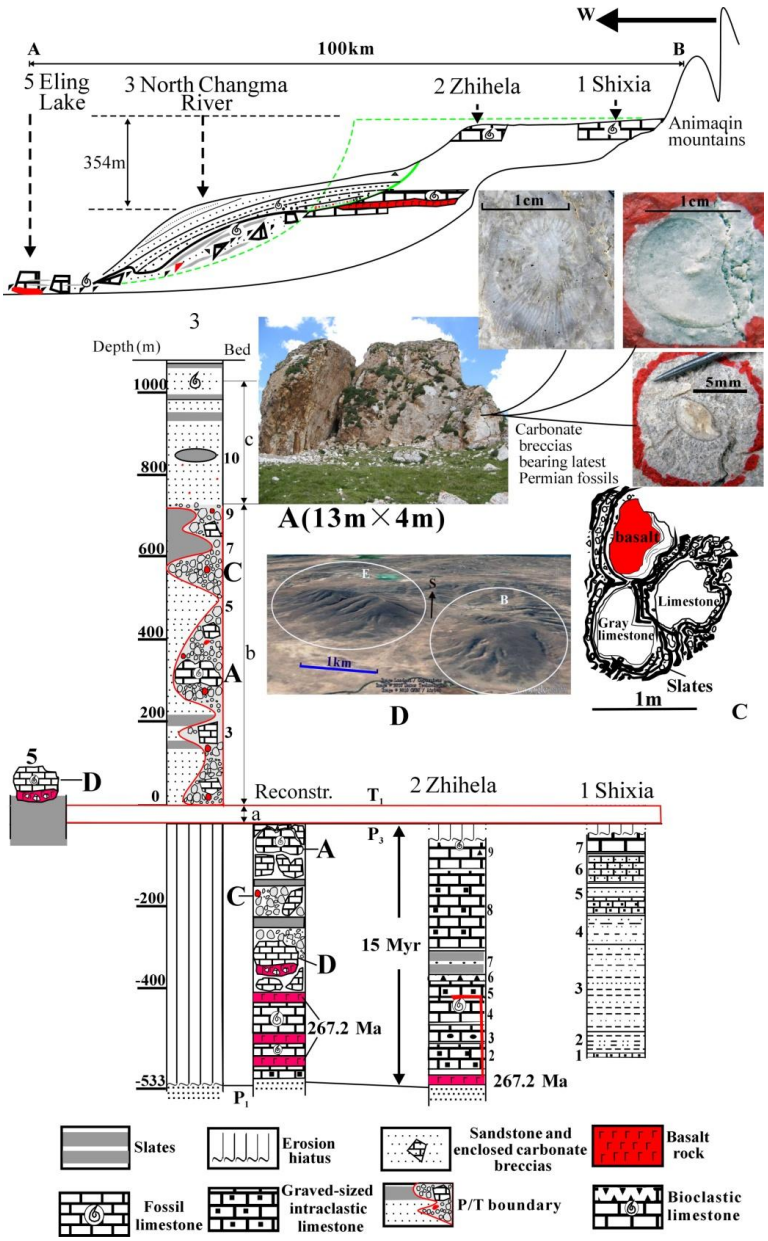

Figure 5. Correlation of series PTB sections 1, 2, 3, 5 along with the profile A-B (Figure 4C) from shelf to basin center areas and a reconstructed Permian sequence representing the missing strata of section 3 are displayed. Numbers lines (a to c) mean a period of sea-level drop (extinction hiatus), sea-level low-stand, and sea-level rise, respectively, as shown in Fig.1. A. a photo of giant carbonate collapse (size:13m×4m) bearing the uppermost Permian corals, ammonites, and brachiopods embedded in a matrix of early Triassic siltstones or slates; C. wave-polished conglomerates reworked from a carbonate platform, are enclosed in black slates and siltstones, containing one basalt and two fusulinid-bearing carbonate boulders. D. two kilometer-sized megabreccias (B, E) bearing mid-Permian fusulinid assemblages on google maps 35°03′18.97″N, 97°57′54.22″E with an angle of view altitude 5.7km.

4.5 Eling lake section[38]

The Triassic carbonate bioclasts, kilometer-sized mage-breccias [Figure 5D] bearing the middle Permian fusulinids overlaid Late Permian siliceous slates. Siltstones intercalated with mudstones bear radiolarians *Pseudoalbaillella scalprata*, *Pseudoalbaillella globosa*, and

Pseudoalbaillella scalprata postscalprata.

4.6 Xiadawu section(34°55′N, 99°15′E)[28][page 59]

The sequence [Figure 2D] shows a coarsening-upward character, from deep-water slates with a small amount of thin-bedded sandstones (Beds 5-7, 753 m) to coastal polymictic conglomerates (Bed 8, 364 m). The overlying volcano (Beds 9-14, 752m) contains two complete breccia-tuff-basalt cycles (breccia Bed 9, 91.74 m; tuff Bed 10, 58.24 m; basalt Bed 11, 59.18 m; breccia Bed 12, 52.59 m; tuff Bed 13, 26.4 m; basalt Bed 14, 463.6 m; no overlying strata). The volcano's upper age limit is constrained at 247.2 Ma by its overlying fossils, *Nicomedites*, *emiornites*, *Septaliphoria xingyiensis*, *Pseudospiriferina tsinghaiensis*, *Koeveskallina media*, *Pseudospiriferina tsinghaiensis*, *Abrekia* cf. *applanata*. Twenty single zircon ages from a 3-meter-thick tuff bed[30] of Bayan Har Group on the west side of Xiadawu Volcano show a longer span between 254±2 and 242±1 Ma, indicating Xiadawu Volcano was synchronous with Siberian Traps volcanism.

5. Evidence supporting the end Permian marine regression

5.1 Carbonate megabreccias deposited on slopes and along basin margins

Carbonate megabreccias occur as lowstand features[52]. Widespread carbonate breccias [Figure 8.1-6] are reworked from the Permian platform, ranging from millimeters to kilometers. The sections in North America and the Canadian Rockies correlated perfectly with those in Arctic Canada[23], Oman[2], Chinese Bayan Har basin, where the last 15-Myr Permian strata were missing during the oldest Triassic times [Table 2]. The regression-related EPME postdates the uppermost Permian shallow shelf or deep-water shale sequence [Figure 2D] and predates the conglomerates or carbonate breccias.

5.2 The PTB sequences show a coarsening-upward character

The Xiadawu and North Changma River sections display sequence changes from marine shales to coastal conglomerates. Xiadawu section witnessed an uplift-erosion-basalt process, following the rule of Campbell's plume theory[29].

In Penglaitan[9], South China, the uppermost Permian Bed 141 coarsening upward from limestone to sandstones indicates platform shallowing. Due to the deposition conditions changed sharply, a hiatus should occur between Beds 141and 142, consistent with severe marine regression. The resultant isolated or semi-isolated basin was indicated by a terrestrial

input of freshwater and plant matter, as suggested by the occurring of euryhaline organisms in organic-rich black shale and thin-bedded limestone in Bed 142.

Closure of the Paleo-Asian Ocean or collision between Siberia and North China has confirmed a severe regression across the PTB. The transition suggests this sea-level drop from the deep-water marine deposition of upper Permian Linxi Formation to continental gravel sandstone, non-marine slates, and tuffs with zircon ages 252±1.7 Ma or 249.9±1.6 Ma, of the lowest Triassic Xingfuzhilu Formation[53].

5.3 The sediment surge over tens of times, as indicated by a sharp increase in $^{87}Sr/^{86}Sr$[Figure 6]

Table 1. A sharp increase in deposition rate across the PTB interval in the study localities

The study localities	beginning (Ma)	end (Ma)	Thickness(m)	Deposition rates (m/Ma)
Donggeicuona Lake[41]	251.94	228	13280	554.72
South Zone[31]	251.94	245	5154.38	742.71
North Zone[31]	251.94	245	3424.67	493.47
North Changma River	251.94	251.3	1078	1684.38
ZHihela section	267.2	251.94	417.52	27.36

The considerable thickness of accumulation and high deposition rate [Table 1] strongly supports the end-Permian marine regression during the early-Triassic interval. The large-scale collapses of carbonate platforms and granite excursion through the tensile transition zone between continental margin and ocean have proved the east continental pre-magmatic uplift and the west deepening of the oceanic bottom.

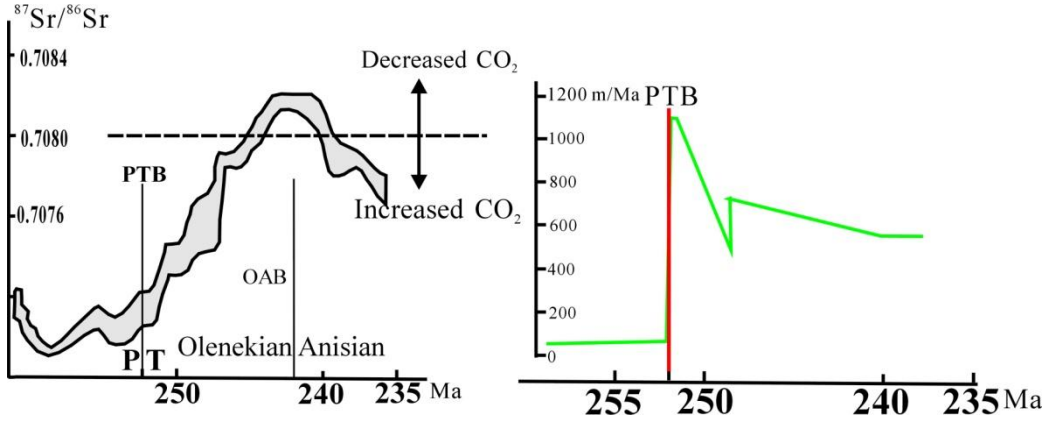

Figure 6. The apex of the long-term $^{87}Sr/^{86}Sr$ curve[34, 54] (left) shows a 10-Myr lag after the peak of the average deposition rate curve (right) across the PTB. Left: the 1-Ma step $^{87}Sr/^{86}Sr$ curve with peak values occurred at the Olenekion-Anisian boundary, a 10-Myr-long lag after the PTB. Right: green curve shows the average deposition rate, the blond bar showing the extinction interval when the sea-level dropped sharply, and the resultant deposition rate increased dramatically.

5.4 The granite intrusions

Uplift of the continental platform or deepening of the basin bottom intensified the tensile state at the shelf edge, where witnessed the granite intrusions at 251.0±0.8 Ma[41] between the oversteepened carbonate wall and the high angle slope in Qingshui Spring, East Kunlun Mountains. Oversteepening and abnormal thickening of the wall benefited from the long-lasting subsidence of the passive continental platform and exuberant growth of organisms, coupling with the end-Permian regression, which led to a lack of seaward confining stress. Leading tensile stress in the middle of the platform shelf ultimately triggered the submarine gravity-driven sliding and generated large quantities of megabreccias.

5.5 Global regression signals

Most carbonate sediments and coal of the late Paleozoic (the most famous coaling period) were subjected to erosion by the sea-level falls of hundreds of meters, resulting in negative global excursions in carbon isotopic $\delta^{13}C$[12, 55-57] [35, 58],[57](Figure 10).

A sharp increase in ratios of $^{87}Sr/^{86}Sr$ [34, 35, 56, 57], intensified weathering[5, 35], climate change from humid to arid [18, 35], continentalization, desertification, wildfires[13], or drought enhanced terrestrial input[37] and anomalous marine sediment fluxes[36, 37]. Restriction events within the Paleotethys ocean[59], Tibetan-sized plateaux[60] in supercontinent Pangaea, and an estimated change of sea-level 400-650 m[61], as well as a minimum shallow-water area of 13%[20] during the latest Permian, are all marine regression signals.

6. Discussion

6.1 Submarine carbonate collapse, and why "nappes" or "palaeo-seamounts" are untenable

Changma River Formation is characterized by the widely distributed mm- to km-sized carbonate clasts embedded in a matrix of mainly dark slates intercalated with sandstones. The giant breccias have received various interpretations of tectonic-driven[62] or mid-Permian palaeoseamounts[38]. Thanks to the application of Google Maps and 3D image scanning, various sea-floor morphological features of sediment redistribution have been recognized [63-66]. The new technologies have given us a new understanding of the previous regional survey data[31]. These mound-like carbonate hills [Figure 5A, 5D; Figure 8.3, 8.5, 8.6] distributed chaotically and moved independently from one another [Figure 4C], with syn-depositional bedding [Figure 8.6], showing rootless features and no tectonic

characteristics. Consequently, they couldn't be the "nappes" formed during the orogenesis stage[62]. So-called middle Permian palaeoseamounts[38] are, in fact, of km-sized megabreccias because the shallow-water carbonate seamounts couldn't grow in basin center areas with a depth greater than 1500 m[38], and the benthic organisms on the palaeo-seamounts couldn't live on an aphotic sea-floor. It is speculated that the palaeo-seamounts may have been reworked from carbonate platforms during the end Permian regression (should be of earliest Triassic Age) due to their similar bio- and lithostratigraphy of the strata.

6.2 The synchrony between the regression and the onset of carbonate collapse

Global sea level controls the growth of carbonate platforms[67]. The sea-level rise created more accommodation spaces, and carbonate platforms grow upward and keep up with the level. When sea level drops, carbonate platforms are exposed to erosion until the platforms' height decreased to sea level. Given the collapse had occurred at an earlier time (e.g., at 253 Ma), a drowning event would occur, leaving the truncated scar in an aphotic zone without new carbonate growth. Or new carbonate deposits would fill in the scar-related depression in a euphotic area through an interval of less than ~1 Myr-long applied by accumulation rates of 200 m/Ma[67]. The filling of the wall scar would continue to grow upward because the long-lasting subsidence at the passive continental margin created an accommodation space until the falling water-level restricted the sediment production at 251.94 Ma end-Permian global regression initiated. Therefore, the carbonate collapse was triggered at 251.94 Ma and was coeval with the onset of global regression.

6.3 Debates focusing on the end Permian regression

Many authors[3, 4, 6, 8, 9, 58] deny the end-Permian regression due to its continuous PTB sequences or ascribe the end-Permian hiatus to submarine erosion [Fig. 7below], even think "latest Permian……coincides with a major transgression" [3].

The so-called continuous sequences are, in fact, of freshwater deposits rather than marine sediments. The Wujiapingian-Changhsingian boundary of late Permian recognized a global regression of sea level [3, 23]. The shallow-water sedimentary structure (equivalent to Bed 8 of the Zhihela section) of the storm deposits suggests a water depth of 30~50 m. This paper also admits this late Permian regression. But it didn't result in the widely distributed bioclasts because of some bearing the latest Permian fossils [Fig. 5A, Fig. 8.3,8.4]. Moreover, the

thickness of the earliest Triassic (Griesbachian) turbidite sequence ranges up to more than 1 km in the basins of Chinese Bayan Har (North Changma River section, 1087m) and Canadian Sverdrup[23]. How could the late Permian basins with 50-meter deep in distal center areas accommodate up to 1 km thick sediment?

Intensified weathering[5, 35], climate change from humid to arid [18, 35], enhanced terrestrial input[37], anomalous marine sediment fluxes[36, 37] wouldn't be the results of the hot climate. Can the hot weather produce giant carbonate blocks ranging from hundred meters to kilometers [Fig. 5D, Fig. 8.1, 8.2, 8.5, 8.6], which were reworked from Permian platforms and embedded in a matrix of earliest Triassic slates, siltstones, and sandstones? Abraded bioclasts that occurred in strata of later Griesbachian[3] may result from re-delivery and redeposition from the earliest Triassic regression unit (equivalent to Bed 10 of the Zhihela section).

Tab.2 The last 15-Myr Permian unrepresented by strata in north Pangea (Canadian Arctica[1], Oman[2])

North Pangea Basin Margin			Canadian Arctica	Oman	This Paper
Lower Triassic			BJ	Aseelah Unit	CMR FM
Permian Upper	Changhsingian	Subaerial erosion			
Permian Upper	Wuchiapingian	Subaerial erosion			
Permian Middle	Capitanian	Subaerial erosion			
Permian Middle	Wordian	Submarine erosion	TF DE	Qarari Unit	MEZ FM
Permian Middle	Roadian	Submarine erosion			
Permian Lower	Kungurian	Submarine erosion			
Permian Lower	Artinskian	Submarine erosion			

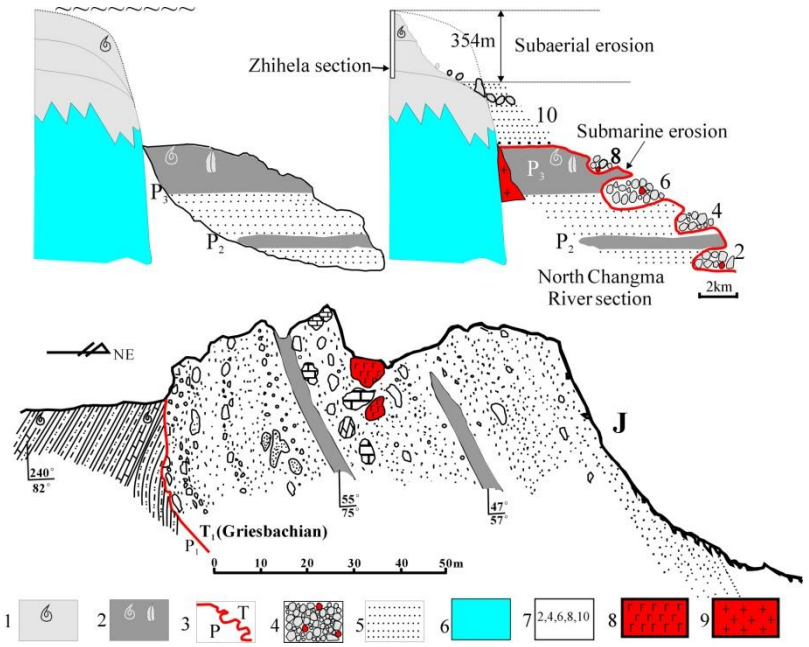

Figure 7. The above shows subaerial erosion and submarine erosion. The below shows a submarine-erosion unconformity separating the lower Permian from the overlying Lower Triassic at the shelf edge. Legends: (1) Latest Permian limestone ammonoid, (2) Shale bearing Changhsingian conodonts, (3) P/T boundary, (4) Conglomerates, (5) Sandstone, (6) Carboniferous-Permian sequences, (7) Bed No. in North Changma River section, (8) Basalt, (9) Granite 251.0±0.8 Ma.

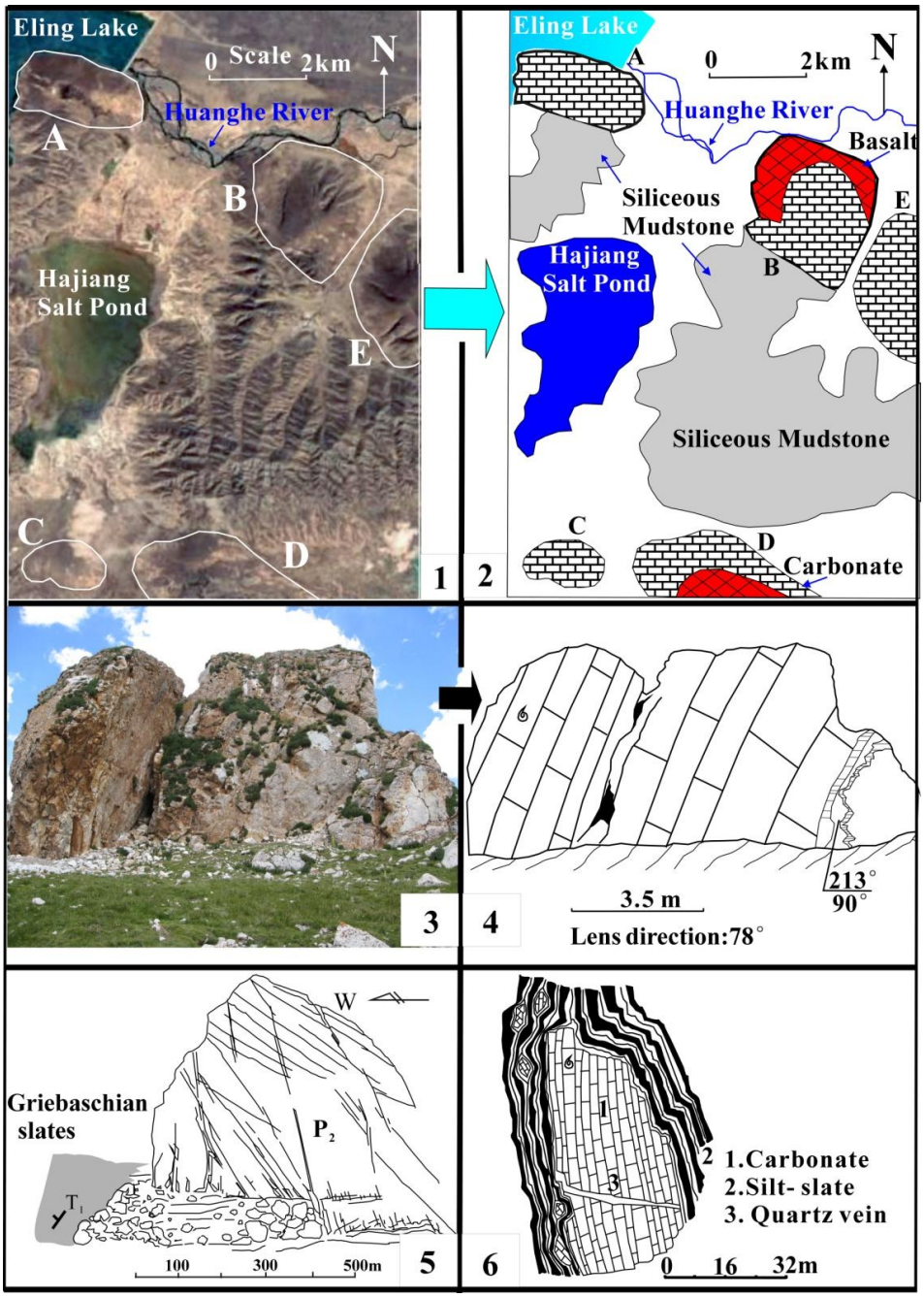

Figure 8. Outcrops of rocks on google maps or photos. An illustration (**1**) showing the five megabreccias (A to E) near Eling Lake (B and E are the same with Figure 5D) on google maps 35°03′18.97″N, 97°57′54.22″E with an angle of view altitude of 5.7km, and their corresponding geological sketch (**2**) after[38], the red color is showing basalt rocks; **(3)** a photo of uppermost Permian carbonate collapse, lens direction: 78°, stratigraphic occurrence: 213°∠90°, location: 34°18′46.8″N, 99°26′57.7″N, H 4410 m, and its related geological sketch (**4**); a photo **(5)**

showing a mid-Permian fusulinid-bearing mound carbonate block enclosed by early Triassic slates; **(6) a** giant carbonate breccia surrounded by Early Triassic (Griebaschian) slates.

7. Calibrating the magnitude of global regression

Three steps to calibrate the magnitude of global regression:

7.1 To reconstruct the Permian sequence eroded

Detailed fossil ranges [Figure 3] in the study area suggested a continuous faunal succession of Permian and early Triassic age. In contrast, an unconformity separating the lower Permian from the overlying lower Triassic [Fig. 7below] represents most of the PTB sections [Figure 4B, I-V] along the passive continental margin in the Bayan Har basin. The mid-to-upper Permian strata were eroded both submarine and subaerial and are reworked in conglomerates [Fig.5C], or mound collapsed breccias [Figure 5A] embedded in a matrix of early Triassic dark shales, siltstones, or sandstones.

Liangshanophyllum occurred in Changma River [Fig.5A] and Donggeicuona Lake[41]. *Huayunophyllum* in the south edge of East Kunlun[39, 41], the joint occurring of *Waagenites barusiensis* and *Palaeofusulina globosa* in Shixia[43, 44], and *Iranophyllum* in Zhihela and West Changma River[31]that occurred in very late of Changhsingian[68] reconstructed the uppermost Permian sequence. The mid-Permian horizon is reconstructed from the reworked fusulinid-bearing megabreccias[Fig. 8.1][38] in Eling Lake, or from limestone beds intercalating with basalts of Maerzheng Formation in Maya section[Fig.4C].

7.2 To correlate the reconstructed Permian sequence with the Zhihela section

In the Zhihela section, two regression Beds: (Wujiapingian?-Changhsingian) Bed 8 and the earliest Bed 10 intercalated the transgression Bed 9 bearing the uppermost Permian fossils (*Iranophyllum* occurred until very late in Changhsingian[68]). A mound-like carbonate breccia [Fig. 5A] is reworked from Bed 9, indicating that the end Permian regression (Bed 10) is responsible for the widely distributed bioclasts rather than the previous one (Bed 8). From a high diversity of benthic fauna in Bed 9 to a complete disappearance of biota in Beds 10 indicates EPME occurring between them because an occurrence of gastropods in Bed 11 suggests the certainty of early Triassic age[9, 17, 69] (e.g., 242 Ma), which occurred in South China.

Mid-Permian fusulinid-basalt zone is crucial to determine the magnitude of sea-level drop.

Two giant blocks reworked from the mid-Permian fusulinid strata. One occurred in situ [Fig. 8.5] through subaerial erosion, another formed through submarine erosion and redeposited in distal basin center areas[Fig. 5D, Fig. 8.1, 8.2]. Subaerial and submarine erosions aren't mutually exclusive[Fig. 7above]. How much the sea-level drop or the thickness-equivalent strata eroded through subaerial erosion is difficult to determine. The wave base may have reached the fusulinid-basalt zone because the round, water-polished fusulinid-basalt-bearing boulders or pebbles show subaerial characters [Fig. 5C], but fusulinid-bearing limestones intercalated with basalts with ages of 267±5.3 Ma or 267.2±3.4 Ma[28] preserved well in a mid-Permian sequence of Maerzheng Formation, in Aliza, and Yama[Fig.3C][31].

7.3 To calibrate the magnitude of global regression[Fig. 5] [Fig. 9]

The last 15-Myr Permian shallow-water platforms were eroded not only in Chinese Bayan Har but also in Canadian Arctica[1], Oman[2], Canadian Rockies[3], Norway[3], North America[3] all over the world. A global sea-level drop of at least 354 m is deduced by correlating with Beds 5-9 of the Zhihela section, whereas Beds 2-4 or previous strata eroded through submarine erosion[Table 2]. Although this magnitude calibration is speculative due to the large ranges in thickness of the fusulinid-basalt zone, it is consistent with the regional doming of 364 m indicated by the Xiadawu section [Fig.2D] from deep ocean shale Beds 5-7 to coastal conglomerate Bed 8. The latest papers have verified this magnitude calibration, "***the amplitude of end-Permian sea level drop is at least 190 m in Sichuan Basin***" [70] and "***restriction events within the Paleotethys ocean***" [59].

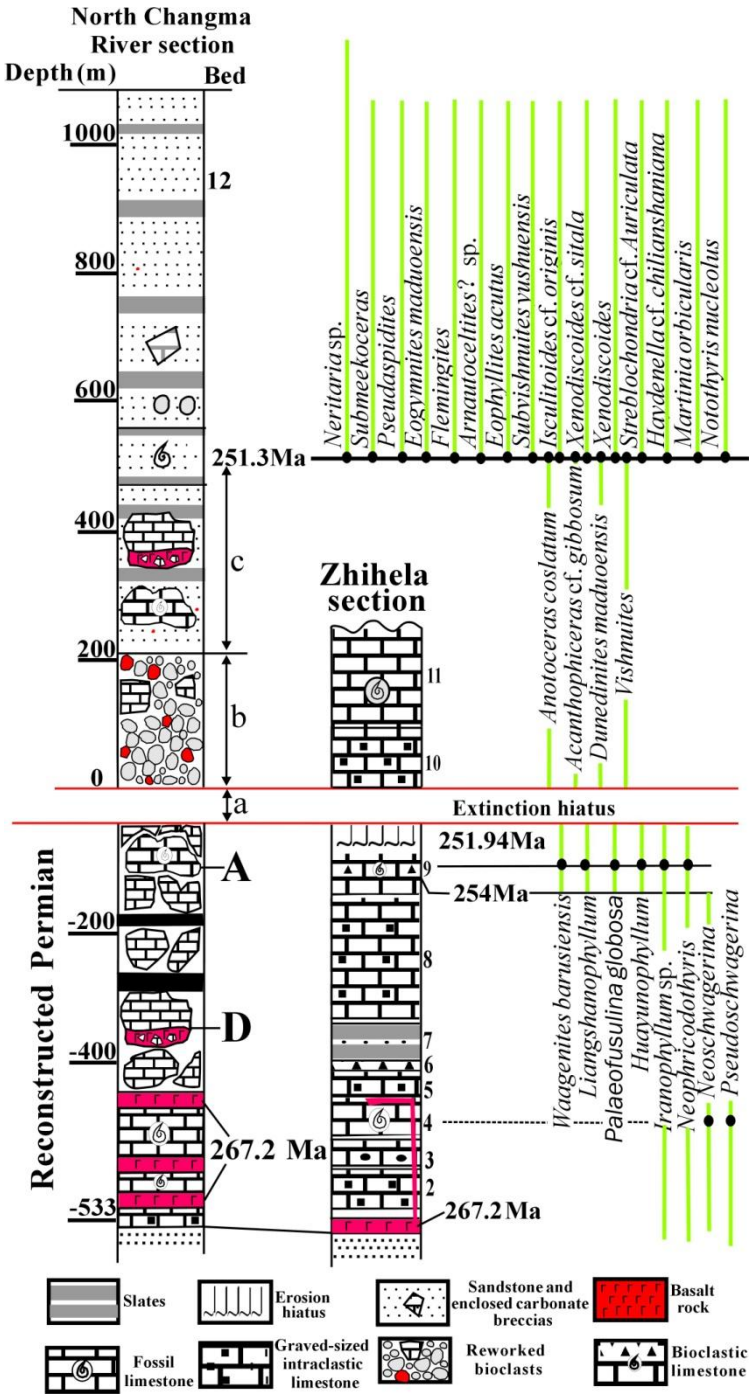

Figure 9. Correlation between the reconstructed Permian biostratigraphic sequence and the measured Zhihela across the PTB interval shows that a sea-level drop of 354 m led to erosion of the last 15-Myr Permian strata as thick as 533 m during the end-Permian regression. Numbered lines (a to c) represent a period of sea-level drop (extinction hiatus), sea-level low-stand, and sea-level rise or volcanic eruptions, respectively, as shown in Fig.1. A and D are magebreccias showing in Figure 5. A, D.

Conclusion

Our geological sections demonstrate three discoveries: 1) a global sea-level drop of 354 m; 2) the period of extinction falls within the hiatus, representing the duration of sea-level drop; 3) Siberian Traps volcanism, global warming, anoxia, and ocean acidification are all post-extinction events.

Why did the extinction occur during the falling stage? We will never know because we can't study a hiatus unrepresented by strata unless we associate the extinction with the sea-level drop, which reduced the shallow-water habitat regions to a minimum. The severe marine regression and the resultant drought also killed land plants and animals. The study of the past helps to protect the human future. The global threat to human security could be habitat loss rather than global warming, although global warming could also cause habitat loss.

REFERENCES CITED

1. Thorsteinsson, R., *Carboniferous and Permian stratigraphy of Axel Heiberg Island and western Ellesmere Island, Canadian Arctica Archipelago.* Geological Survey of Canadian Bulletin, 1974. **224**: p. 1-115.
2. Hauser, M., D. Vachard, and R. Martini, *The Permian sequence reconstructed from reworked carbonate clasts in the Batain Plain (northeastern Oman).* Earth and Planetary Sciences, 2000. **330**: p. 273-279.
3. Hallam, A. and W. P.B., *Mass extinctions and sea-level changes.* Earth-Science Reviews, 1999. **48**: p. 217-250.
4. Bottjer, D.J., *Lethally Hot Temperatures During the Early Triassic Greenhouse.* Science, 2012. **338**: p. 366-370.
5. Cao, Y., H. Song, and T.J. Algeo, *Intensified chemical weathering during the Permian-Triassic transition recorded in terrestrial and marine successions.* Palaeogeography, Palaeoclimatology, Palaeoecology, 2019. **519**: p. 166-177.
6. Song, H., et al., *Anoxia/high-temperature double whammy during the Permian-Triassic marine crisis and its aftermath.* Scientific Reports, 2014. **4**(4132): p. 1-7.
7. Penn, J.L., et al., *Temperature-dependent hypoxia explains biogeography and severity of end-Permian marine mass extinction.* Science, 2018. **362**(1130): p. 1.
8. Joachimski, M.M., A.S. Alekseev, and A. Grigoryan, *Siberian Trap volcanism, global warming and the Permian-Triassic mass extinction: New insights from Armenian Permian-Triassic sections.* GSA Bulletin, 2020. **132**(1-2): p. 427-443.
9. Shen, S., J. Ramezani, and J. Chen, *A sudden end-Permian mass extinction in South China.* GSA Bulletin, 2019. **131**(1-2): p. 205-223.
10. Payne, J.L., et al., *Calcium isotope constraints on the end-Permian mass extinction.* PNAS, 2010. **107**(19): p. 8543-8548.
11. Wignall, P.B. and R.J. Twitchett, *Oceanic anoxia and the end Permian mass extinction.* Science

1996. **272**(5265): p. 1155-1158.
12. Clarkson, M.O., et al., *Ocean acidification and the Permo-Triassic mass extinction.* Science 2015. **348**(6231): p. 229-232.
13. Shen, S.-z., et al., *Calibrating the End-Permian Mass Extinction.* Science, 2011. **334**(1367): p. 1367-1372.
14. Burgess, S.D., S. Bowring, and S. Shen, *High-precision timeline for Earth's most severe extinction.* PNAS, 2014. **111**(9): p. 3316-3321.
15. Fu, X.G., J. Wang, and C.Y. Song, *The Permian-Triassic transition in ocean island setting: Environmental disturbances and new high-resolution carbon-isotope record from the Qiangtang Basin, NW China.* Palaeogeography, Palaeoclimatology, Palaeoecology, 2019. **522**: p. 40-51.
16. Tian, L., et al., *Environmental instability prior to end-Permian mass extinction reflected in biotic and facies changes on shallow carbonate platforms of the Nanpanjiang Basin (South China).* Palaeogeography, Palaeoclimatology, Palaeoecology, 2019. **519**: p. 23-26.
17. Yin, H., et al., *The end-Permian regression in South China and its implication on mass extinction.* Earth-Science Reviews, 2013: p. 1-15.
18. Baresel, B., et al., *Timing of global regression and microbial bloom linked with the Permian-Triassic boundary mass extinction: implications for driving mechanisms.* 2017. **7**(43630): p. 1-8.
19. Newell, N.D., *Revolutions in the history of life.* Geol. Soc. Am. Spec. Pap., 1967. **89**: p. 63-91.
20. Schopf, T.J.M., *Permo-Triassic extinctions: relation to sea-floor spreading.* Journal of Geology 1974. **82**: p. 129-143.
21. Hallam, A. and J.M. Cohen, *The case for sea-level change as a dominant causal factor in mass extinction of marine invertebrates*. Biological Sciences. Vol. 325. 1989, Philosophical Transactions of the Royal Society of London. 437-455.
22. Shen, S.-z. and S.A. Bowring, *The end-Permian mass extinction: a still unexplained catastrophe.* National Science Review, 2014: p. 1-4.
23. Grasby, S.E. and B. Beauchamp, *Intrabasin variability of the carbon-isotope record across the Permian-Triassic transition, Sverdrup Basin, Arctic Canada.* Chemical Geology, 2008. **253**: p. 141-150.
24. Stordal, F., et al., *Global temperature response to century scale degassing from the Siberian Traps Large igneous province.* Palaeogeography, Palaeoclimatology, Palaeoecology, 2017. **471**: p. 96-107.
25. Guex, J., S. Pilet, and O. Müntener1, *Thermal erosion of cratonic lithosphere as a potential trigger for mass-extinction.* Scientific Reports, 2016: p. 1-9.
26. Ward, P.D., et al., *Abrupt and gradual extinction among Late Permian land vertebrates in the Karoo Basin, South Africa.* Science, 2005. **307**: p. 709-714.
27. Retallack, G.J. and E.S. Krull, eds. *Carbon isotopic evidence for terminal-Permian methane outbursts and their role in extinctions of animals, plants coral reefs, and peat swamps*. Wetlands Through Time, ed. S.F. Greb and W.A. DiMichele. Vol. 399. 2006, Geological Society of America Special Paper. 249-268.
28. Qinghai Provincial Bureau of Geology and Minerals Exploration and Qinghai Geology Survey Institute, *Geological Map of Qinghai Province (1:1000 000) illustration*, ed. X. Zhang, S. Yang, and Z. Yang. 2005, Beijing: Geology Publication House.

29. Campbell, I.H., *Large Igneous Provinces and the Mantle Plume Hypothesis.* Elements, 2005. **1**: p. 265-269.
30. Zhang, Y.L., et al., *LA-ICP-MS zircon U-Pb ages for dacitic tuffite from Bayan Har Group, northern Tibetan Plateau.* Geological Bulletin of China, 2015. **34**(5): p. 809-814.
31. Bureau of Geology and Mineral Resources of Qinghai Province, *Youyun Commune 1:200,000 Measure Geological*. Regional Geological Survey Report of the People's Republic of China. 1986, Gonghe: Bureau of Qinghai Geology and Mineral Resources.
32. Henderson, C.M., *Uppermost Permian conodonts, and the Permian-Triassic boundary in the Western Canada Sedimentary Basin.* Bulletin of Canadian Petroleum Geology, 1997. **45**(4): p. 693-707.
33. Wignall, P.B. and A. Hallam, *Griesbachian earliest Triassic palaeoenvironmental changes in the Salt Range, Pakistan, and southwest China and their bearing on the Permo-Triassic mass extinction.* Palaeogeogr., Palaeoclimatol., Palaeoecol, 1993. **102**: p. 215-237.
34. Korte, C., et al., *Strontium isotope evolution of Late Permian and Triassic seawater.* Geochimica et Cosmochimica Acta, 2003. **67**(1): p. 47-62.
35. Sun, H., Y. Xiao, and Y. Gao, *Rapid enhancement of chemical weathering recorded by extremely light seawater lithium isotopes at the Permian-Triassic boundary.* PNAS, 2018: p. 1-6.
36. Algeo, T.J. and R.J. Twitchett, *Anomalous Early Triassic sediment fluxes due to elevated weathering rates and their biological consequences.* Geology, 2010. **38**(11): p. 1023-1026.
37. Tian, L., et al., *Rapid carbonate depositional changes following the Permian-Triassic mass extinction: Sedimentary evidence from South China.* Journal of Earth Science, 2015. **26**(2): p. 166-180.
38. Wang, Y., *Structure，and evolution of Middle Permian palaeoseamounts in Bayan Har and its adjacent area.* Science in China Series D: Earth Sciences, 2005. **48**(11): p. 1848-1858.
39. Wang, Y. and H. Yang, *Middle Permian palaeobiogeography study in East Kunlun, A'nyêmaqên and Bayan Har.* Science in China Series D: Earth Sciences, 2004. **47**(12): p. 1120-1126.
40. Wang, Y., G. Xu, and Q. Lin, *Depositional model of early Permian reef-island ocean in Eastern Kunlun.* Science in China, Ser. D, 2001. **44**(9): p. 808-815.
41. Yin, H., K. Zhang, and N. Chen, *Donggeicuona Lake 1:250,000 Measure Geological[M]*. Regional Geological Survey Report of the People's Republic of China. 2001, Wuhan: China University of Geosciences.
42. Zhang, Y.F., *Some opinions about the Triassic stratigraphy in the Bayan Hara area.* Regional Geology of China (in Chinese), 1995(1): p. 21-31.
43. Bureau of Geology and Mineral Resources of Qinghai Province, *Stratigraphy (LithoStratic) of Qinghai Province* Multiple Classification and Correlation of the Stratigraphy of China(63), ed. C. Sun, et al. 1997, Wuhan: China University of Geosciences Press.
44. Liu, G. and X. Li, *The establishment of Danghenanshan Formation and Gequ Formation.* Qinghai Geology, 1994. **3**(2): p. 1-7.
45. Bureau of Geology and Mineral Resources of Qinghai Province, *Regional Geology of Qinghai Province (in Chinese with English Abstract)* 1991, Beijing: Geological Publishing House.
46. Hao, Z. and R. Yu, *The Kunlun-Bayan Har Sea and its relation to evolution of Tethys.* Geological Papers of Qinghai-Tibet Plateau, 1983(4): p. 25-41.
47. Yang, X.D. and X.L. Yan, *New results and major progresses in regional survey of the*

Darlag-Jigzhi sheets. Journal of Geomechanics, 2011. **17**(1): p. 79-90.
48. Province, B.o.G.a.M.R.o.S., *Xiaojin Regional Geological Survey Report*. Regional Geological Survey Report of the People's Republic of China. 1984: Bureau of Sichuan Geology and Mineral Resources.
49. Province, B.o.G.a.M.R.o.S., *Luhuo Regional Geological Survey Report*. Regional Geological Survey Report of the People's Republic of China. 1984: Bureau of Sichuan Geology and Mineral Resources.
50. Yang, H., et al., *Age and general characteristics of calcimicrobialite near the Permian-Triassic boundary in Chongyang, Hubei Province.* Earth Science Journal of China University of Geosciences 2006. **31** (2): p. 165-170.
51. Wang, Y.G., Z.G. Zheng, and C.G. L., *Cephalopoda taxonomic names.* Paleontological Atlas of Northwest China, Qinghai, 1979. **1**: p. 3-59.
52. Haq, B.U. and S.R. Schutter, *A Chronology of Paleozoic Sea-Level Changes.* Science, 2008. **322**(5898): p. 64-68.
53. Zheng, Y.J., F. Su, and F.W. Chen, *New discovery of fossils in the early Triassic Xingfuzhilu Formation, Bairin Right Banner, Inner Monggolia.* Geological Bulletin of China, 2013. **32**(9): p. 1423-1435.
54. Raymo, M.E., *Geochemical evidence supporting T. C. Chamberlin's theory of glaciation.* Geology, 1991. **19**: p. 344-347.
55. WANG, K., H.H.J. GELDSETZER, and H.R. KROUSE, *Permian-Triassic extinction: organic δ13C evidence from British Columbia, Canada.* Geology, 1994. **22**: p. 580-584.
56. Korte, C. and H.W. Kozur, *Carbon, sulfur, oxygen, and strontium isotope records, organic geochemistry, and biostratigraphy across the Permian/Triassic boundary in Abadeh,Iran.* Int. J. Earth Sci., 2004. **93**: p. 565-581.
57. Veizer, J., et al., *87Sr/86Sr, δ13C and δ18O evolution of Phanerozoic seawater.* Chemical Geology, 1999. **161**: p. 59-88.
58. Joachimski, M.M., X. Lai, and S. Shen, *Climate warming in the latest Permian and the Permian-Triassic mass extinction.* Geology, 2012. **40**(3): p. 195-198.
59. Hu, Z., W. Li, and H. Zhang, *Mg isotope evidence for restriction events within the Paleotethys ocean around the Permian-Triassic transition.* Earth and Planetary Science Letters, 2021. **556**.
60. Dewey, J.F. and K.C.A. Burke, *Tibetan, Variscan, and Precambrian basement reactivation: products of continental collision.* J. Geol. , 1973. **81**: p. 683-692.
61. Menard, H.W., *Elevation and subsidence of oceanic crust.* Earth and Planetary Sci. Letters, 1969. **6**: p. 275-284.
62. Wang, G., K. Zhang, and B. Liang, *Texture and tectonic slices of the eastern Kunlun orogenic belt.* Journal of China University of Geosciences, 1997. **22**(4): p. 352-356.
63. Principaud, M., et al., *Large-scale carbonate submarine mass-wasting along the northwestern slope of the Great Bahama Bank (Bahamas): Morphology, architecture, and mechanisms.* Sedimentary Geology, 2015. **317**: p. 27-42.
64. Callot, P., et al., *Giant submarine collapse of a carbonate platform at theTuronian^Coniacian transition:The Ayabacas Formation, southern Peru.* BasinResearch, 2008. **20**: p. 333-357.
65. Pindell, J., R. Graham, and B. Horn, *Rapid outer marginal collapse at the rift to drift transition of passive margin evolution, with a Gulf of Mexico case study.* Basin Research, 2014. **26**: p. 701-725.

66. Nolting，Andrea, et al., *Largest amount of accumulated displacement occurs at the shelf edge at the transition from the vertical reef wall to the upper slope.* Journal of Structural Geology, 2018. **115**: p. 91-102.
67. Bosscher, H. and W. Schlager, *Accumulation Rates of Carbonate Platforms.* The Journal of Geology, 1993. **101**(3): p. 345-355.
68. Wang, X.-D. and X.-J. Wang, *Extinction patterns of Late Permian (Lopingian) corals in China.* Palaeoworld, 2007. **16**(1-3): p. 31-38.
69. Krull, E.S., et al., *Stable carbon isotope stratigraphy across the Permian-Triassic boundary in shallow marine carbonate platforms, Nanpanjiang Basin, south China.* Palaeogeography, Palaeoclimatology, Palaeoecology, 2004. **204**(3-4): p. 297-315.
70. Zhao, R., J. Zhao, and Y. Li, *Amplitude calculation of the end-Permian sea level drop in Northeastern Sichuan Basin, China.* Carbonates Evaporites, 2018. **33**: p. 517-533.

Figures

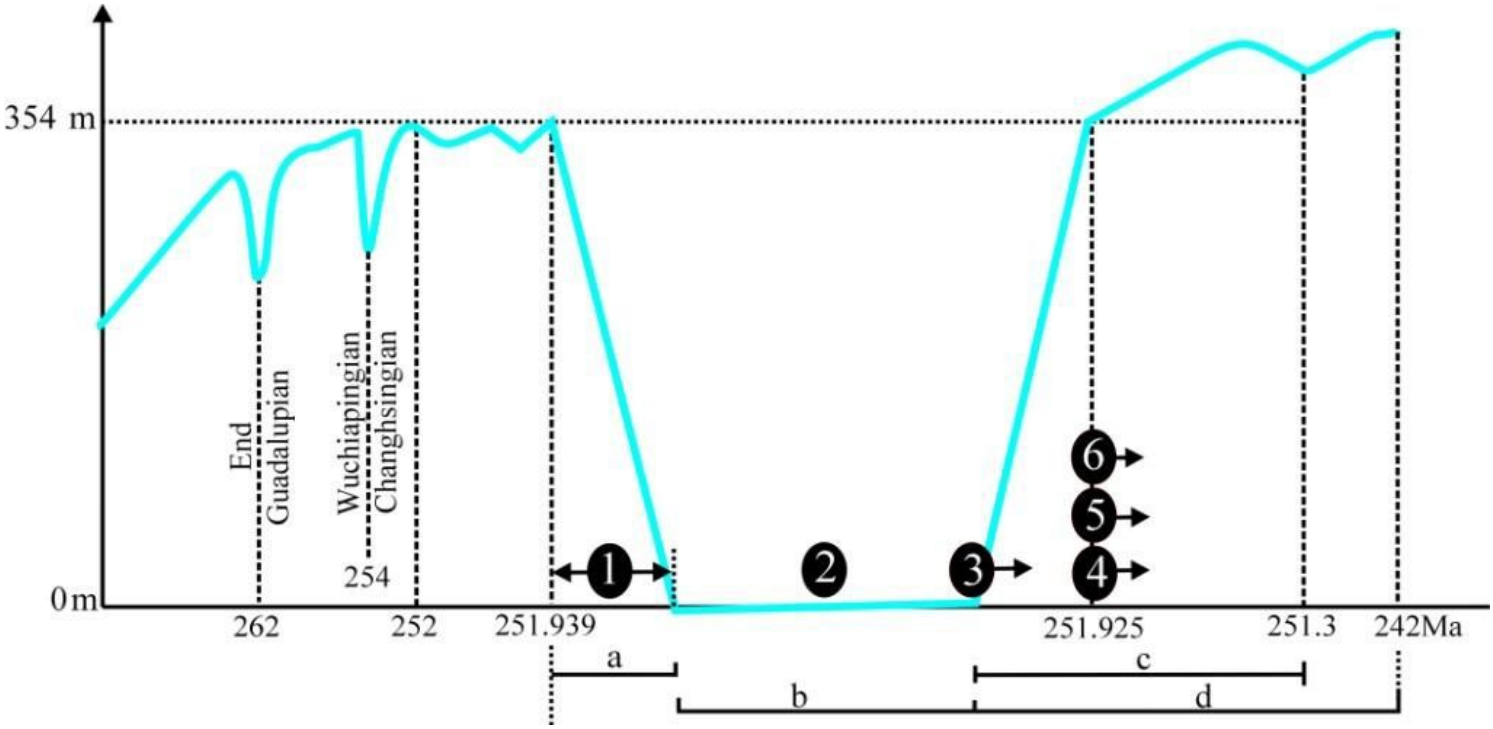

Figure 1

Digitalized geological events (numbered black circles) and the corresponding relative magnitude (green curve) across the PTB interval: (1) extinction event, (2) minimum values of δ13C, (3) initiation of Siberian Traps volcanism, (4-6) onset of warming, anoxia, and ocean acidification, etc.; Numbered lines (a to d) represent a ~3 kyr-long period for sea-level drop (extinction hiatus), ~8 kyr sea-level low-stand, sea-level rise ~0.6 Myr, and volcano eruptions ~10 Myr, respectively.

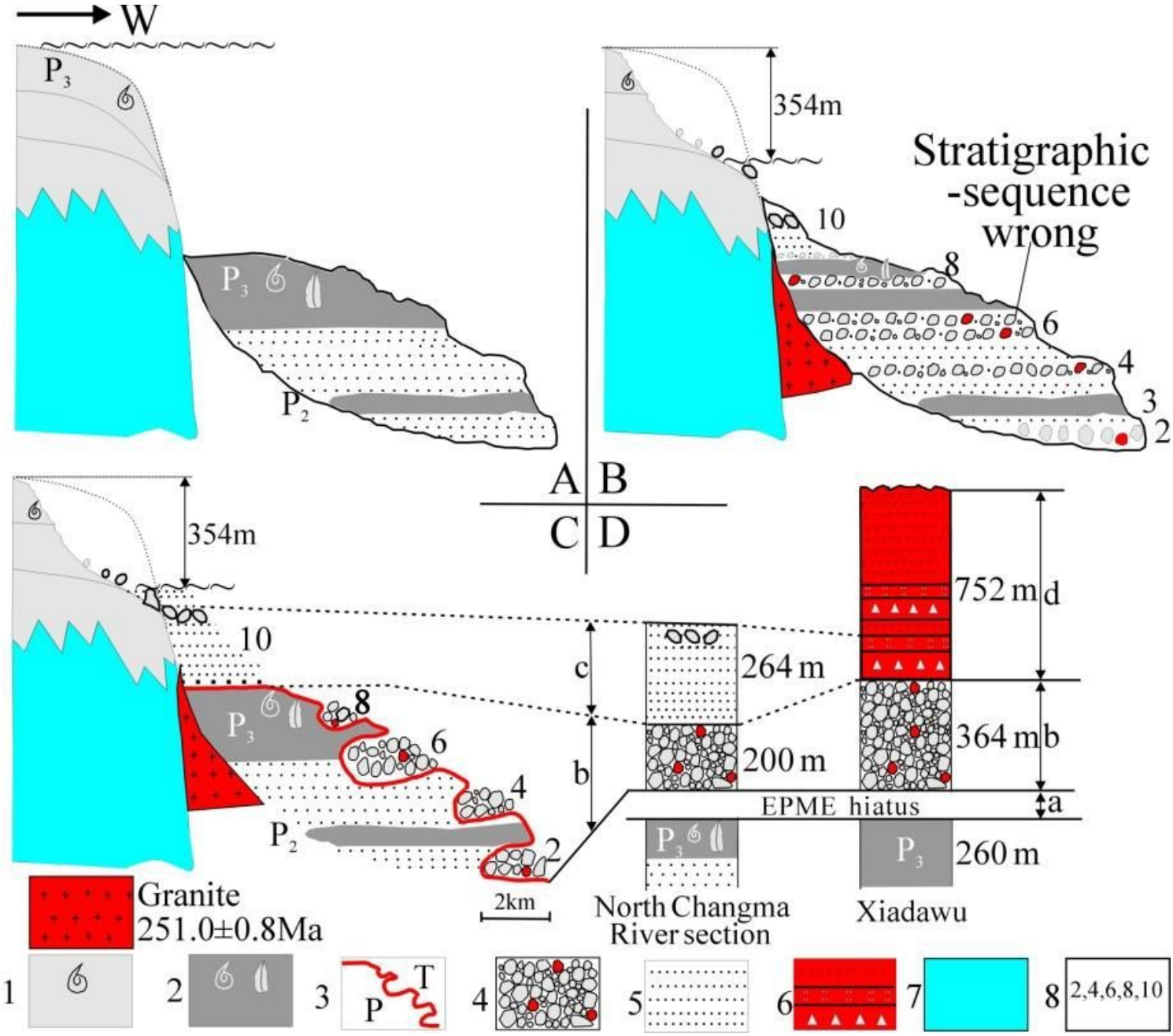

Figure 2

In the North Changma River section, End-Permian faces of shallow-marine and deep-slope are showing before (A) and after (B, C, D) marine regression, as well as a correlation of the PTB sections (D) between North Changma River (left) and Xiadawu (right). Numbered lines (a to d) represent a period for sea-level drop (extinction hiatus), sea-level low-stand, and sea-level rise, as well as volcanic eruptions, respectively, as shown in Fig.1. Legends: (1) Latest Permian limestone ammonoid, (2) Shale bearing Changhsingian conodonts, (3) P/T boundary, (4) Conglomerates, (5) Sandstone, (6) A volcano cycle of breccias-tuff-basalt, (7) Carboniferous-Permian sequences, (8) Bed No. in North Changma River section.

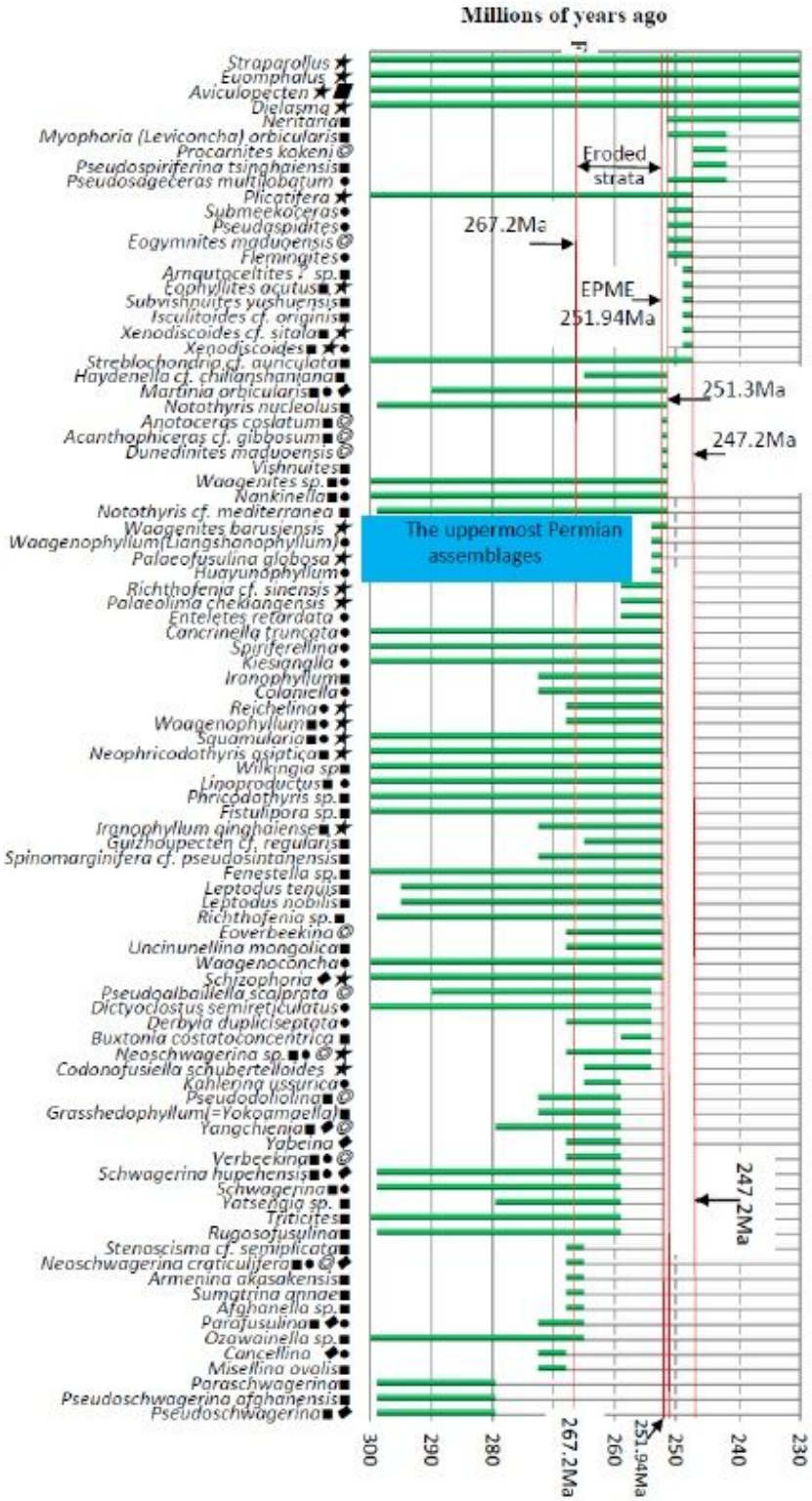

Figure 3

Time-series biostratigraphy across the PTB (~251.94 Ma) interval in the study area; Green-bar is showing the lifespan of the organisms sampled in the studied area based on the database of fossil websites (fossilworks.org); Solid arrows and red lines are dated horizons. The sampling area showing Huashixia (the south slope of East Kunlun[38-40], Donggeicuona Lake[41], Long-Rock Mountains[41]); Changma River[31, 42] (Youyun, Yama);Maduo (Zaling lake paleo-seamounts[38], 24 km eastern Maduo[42, 43]);

Shixia[44, 45] (Maqin town, Zhihela[31], Aliza[31]). A sea-level drop of 354 m results in as thick as 533-m strata were eroded from the uppermost Permian to the basal fusulinid zone, between the two red lines 251.94 Ma and 267.2 Ma. The blue rectangle shows the index fossils of the topmost Permian.

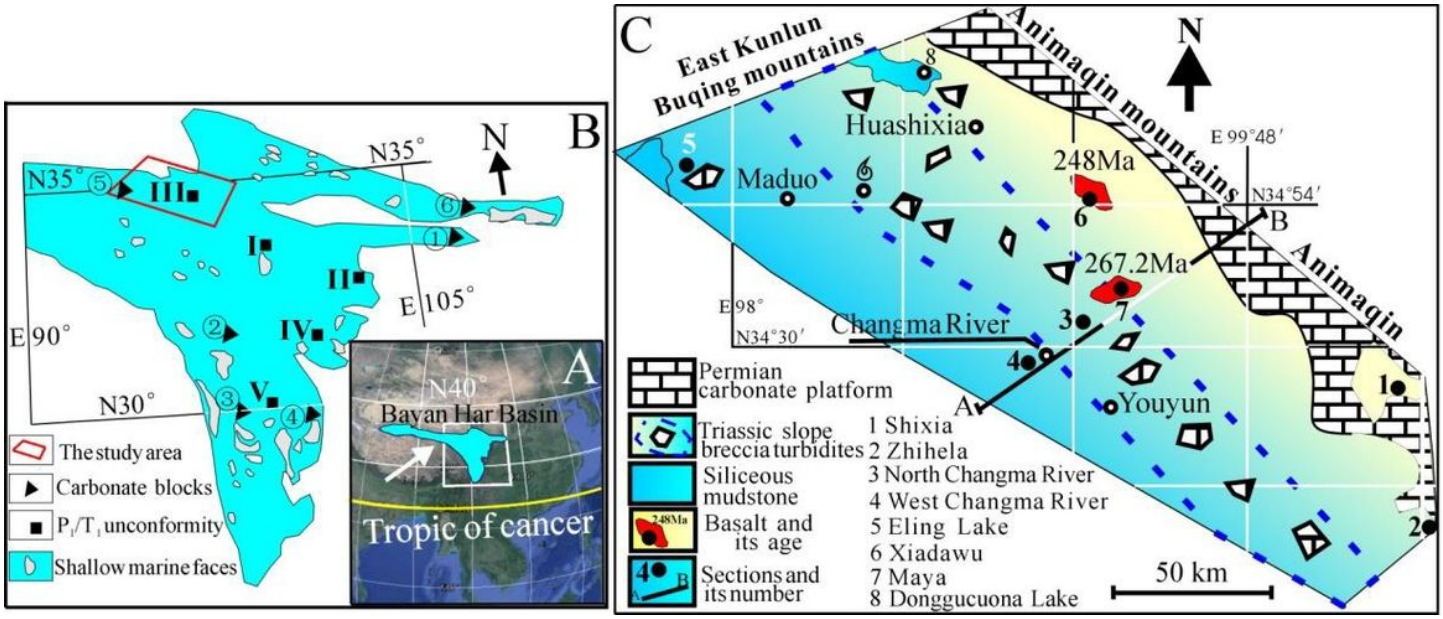

Figure 4

(A) The outline of Bayan Har basin in West China; (B) Paleogeography during the PTB of the Bayan Har Ocean: the red rectangle showing the study area, numbered squares (I to V) are localities representing an erosional unconformity separating Early Permian from the overlying Early Triassic: (I) Mentang[47], (II) Bocigou[48], (III) Changma River[31], (IV) Rilagou[49], (V) Yalong River[42], and numbered triangles (to) [38, 46] are reworked carbonate clasts distributing in Lueyang, Jinsha River, Litang, Ganzi, Eling Lake, Fengxian; and (C) Late Permian to Early Triassic paleogeographic map of the study area: numbered circles (1 to 7) showing the locations of studied sections (1) Shixia, (2) Zhihela in the carbonate platform in the east, and lower-slope (3) North Changma River and (4) West Changma River of early Triassic turbidites in the southwest circled by dashed line enclosing carbonate collapse, (5) Eling Lake in the center basin areas, volcanos of (6) Xiadawu and (7) Yama in the middle study area.Note: The designations employed and the presentation of the material on this map do not imply the expression of any opinion whatsoever on the part of Research Square concerning the legal status of any country, territory, city or area or of its authorities, or concerning the delimitation of its frontiers or boundaries. This map has been provided by the authors.

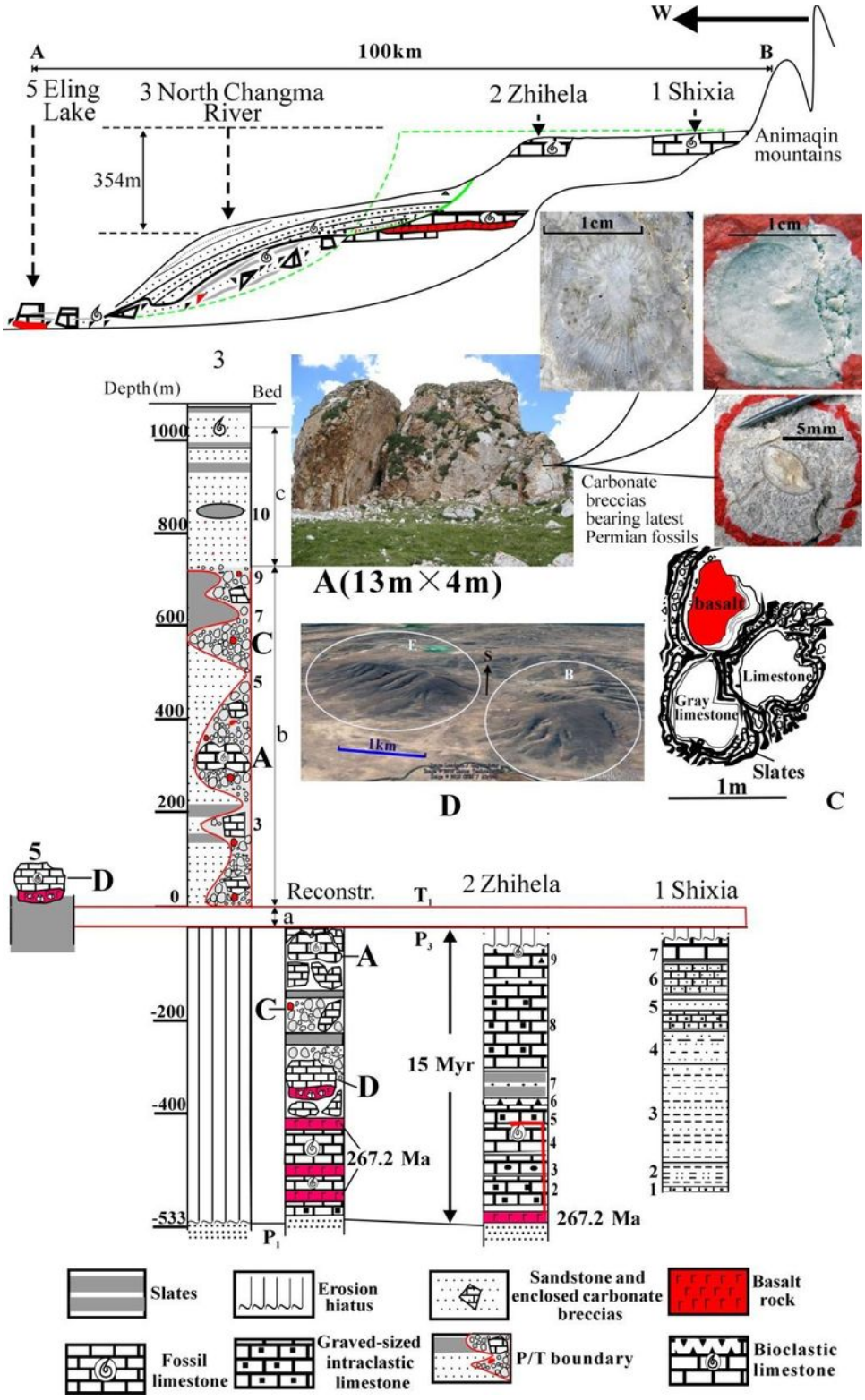

Figure 5

Correlation of series PTB sections 1, 2, 3, 5 along with the profile A-B (Figure 4C) from shelf to basin center areas and a reconstructed Permian sequence representing the missing strata of section 3 are displayed. Numbers lines (a to c) mean a period of sea-level drop (extinction hiatus), sea-level low-stand, and sea-level rise, respectively, as shown in Fig.1. A. a photo of giant carbonate collapse (size:13m×4m) bearing the uppermost Permian corals, ammonites, and brachiopods embedded in a matrix of early

Triassic siltstones or slates; C. wave-polished conglomerates reworked from a carbonate platform, are enclosed in black slates and siltstones, containing one basalt and two fusulinid-bearing carbonate boulders. D. two kilometer-sized megabreccias (B, E) bearing mid-Permian fusulinid assemblages on google maps 35°03'18.97"N, 97°57'54.22"E with an angle of view altitude 5.7km. Note: The designations employed and the presentation of the material on this map do not imply the expression of any opinion whatsoever on the part of Research Square concerning the legal status of any country, territory, city or area or of its authorities, or concerning the delimitation of its frontiers or boundaries. This map has been provided by the authors.

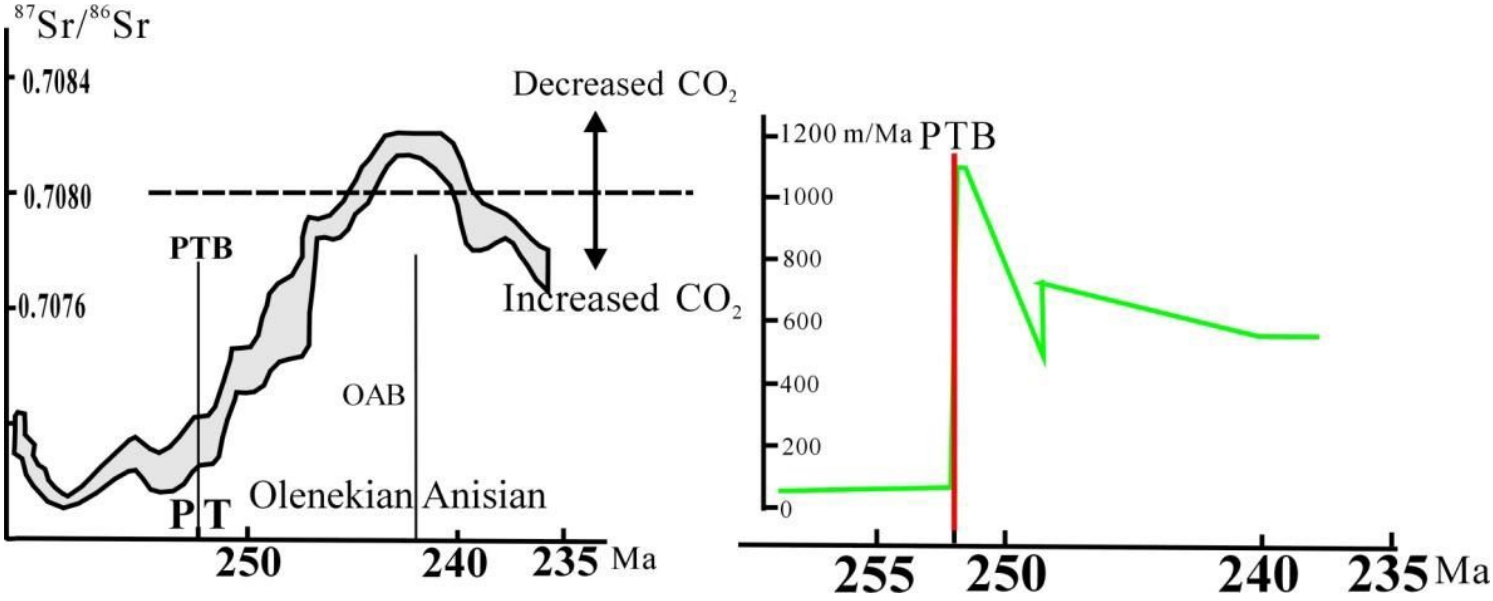

Figure 6

The apex of the long-term 87Sr/86Sr curve[34, 54] (left) shows a 10-Myr lag after the peak of the average deposition rate curve (right) across the PTB. Left: the 1-Ma step 87Sr/86Sr curve with peak values occurred at the Olenekion-Anisian boundary, a 10-Myr-long lag after the PTB. Right: green curve shows the average deposition rate, the blond bar showing the extinction interval when the sea-level dropped sharply, and the resultant deposition rate increased dramatically.

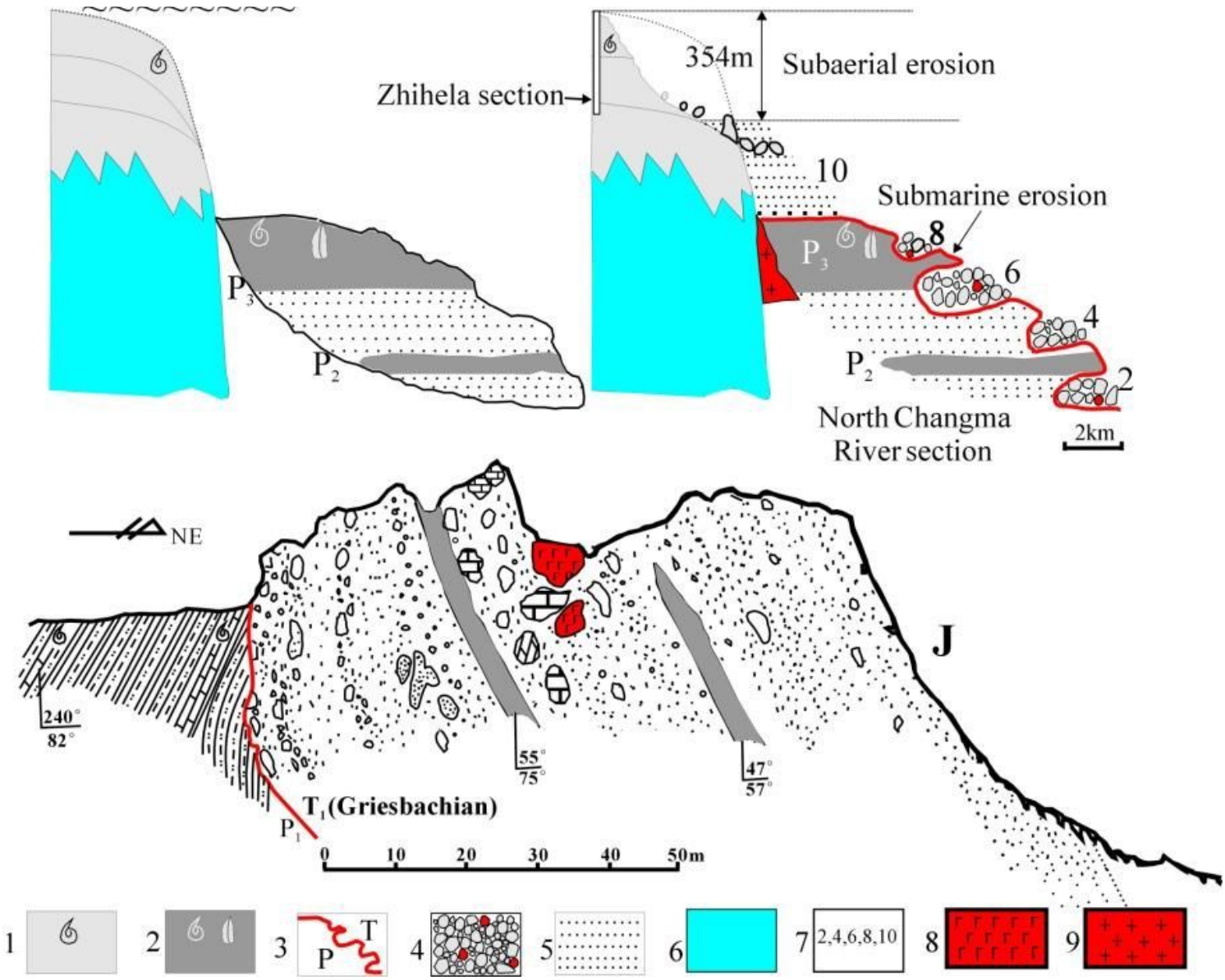

Figure 7

The above shows subaerial erosion and submarine erosion. The below shows a submarine-erosion unconformity separating the lower Permian from the overlying Lower Triassic at the shelf edge. Legends: (1) Latest Permian limestone ammonoid, (2) Shale bearing Changhsingian conodonts, (3) P/T boundary, (4) Conglomerates, (5) Sandstone, (6) Carboniferous-Permian sequences, (7) Bed No. in North Changma River section, (8) Basalt, (9) Granite 251.0±0.8 Ma.Note: The designations employed and the presentation of the material on this map do not imply the expression of any opinion whatsoever on the part of Research Square concerning the legal status of any country, territory, city or area or of its authorities, or concerning the delimitation of its frontiers or boundaries. This map has been provided by the authors.

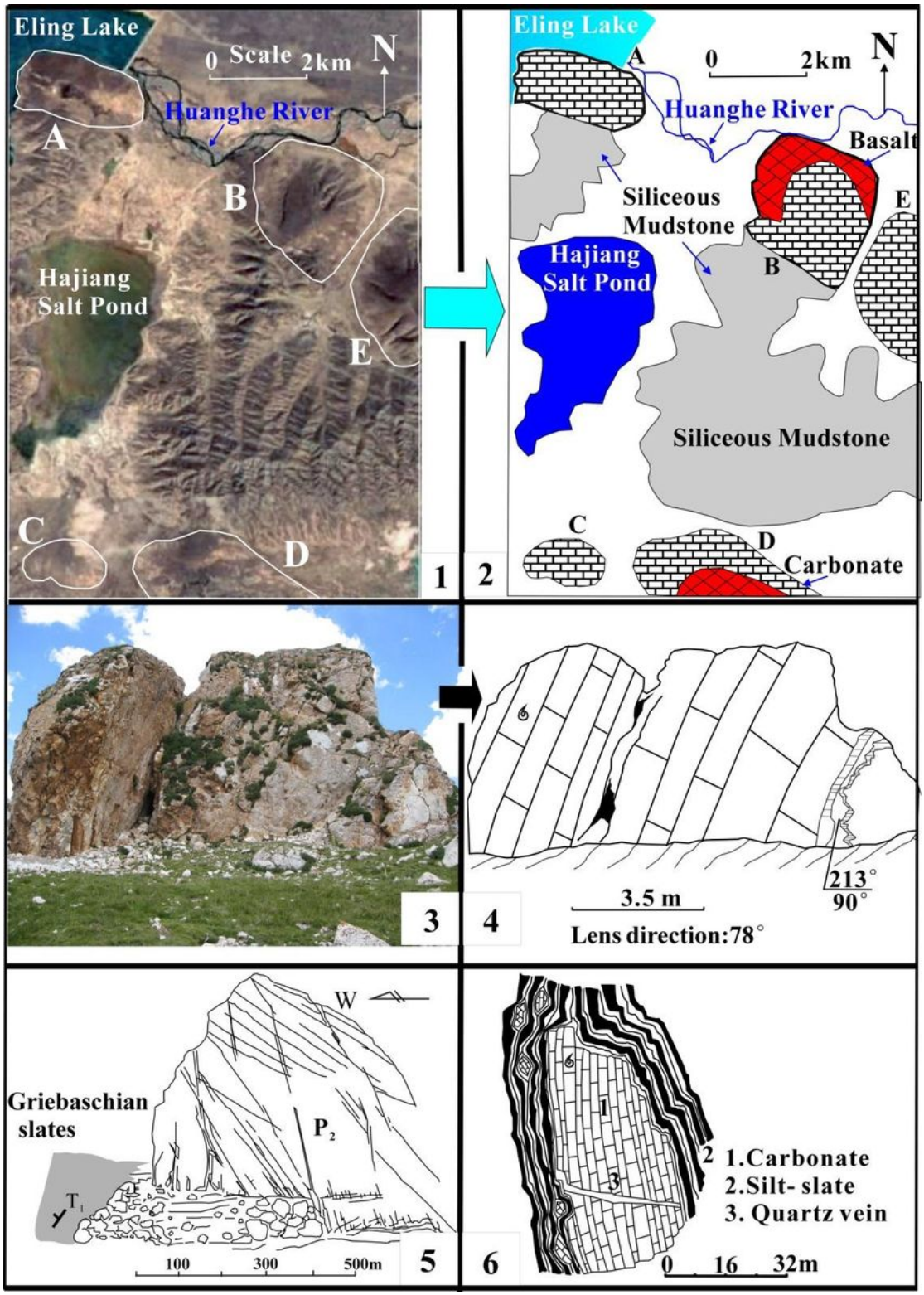

Figure 8

Outcrops of rocks on google maps or photos. An illustration (1) showing the five megabreccias (A to E) near Eling Lake (B and E are the same with Figure 5D) on google maps 35°03'18.97"N, 97°57'54.22"E with an angle of view altitude of 5.7km, and their corresponding geological sketch (2) after[38], the red color is showing basalt rocks; (3) a photo of uppermost Permian carbonate collapse, lens direction: 78°, stratigraphic occurrence: 213°∠90°, location: 34°18'46.8"N, 99°26'57.7"N, H 4410 m, and its related

geological sketch (4); a photo (5) showing a mid-Permian fusulinid-bearing mound carbonate block enclosed by early Triassic slates; (6) a giant carbonate breccia surrounded by Early Triassic (Griebaschian) slates. Note: The designations employed and the presentation of the material on this map do not imply the expression of any opinion whatsoever on the part of Research Square concerning the legal status of any country, territory, city or area or of its authorities, or concerning the delimitation of its frontiers or boundaries. This map has been provided by the authors.

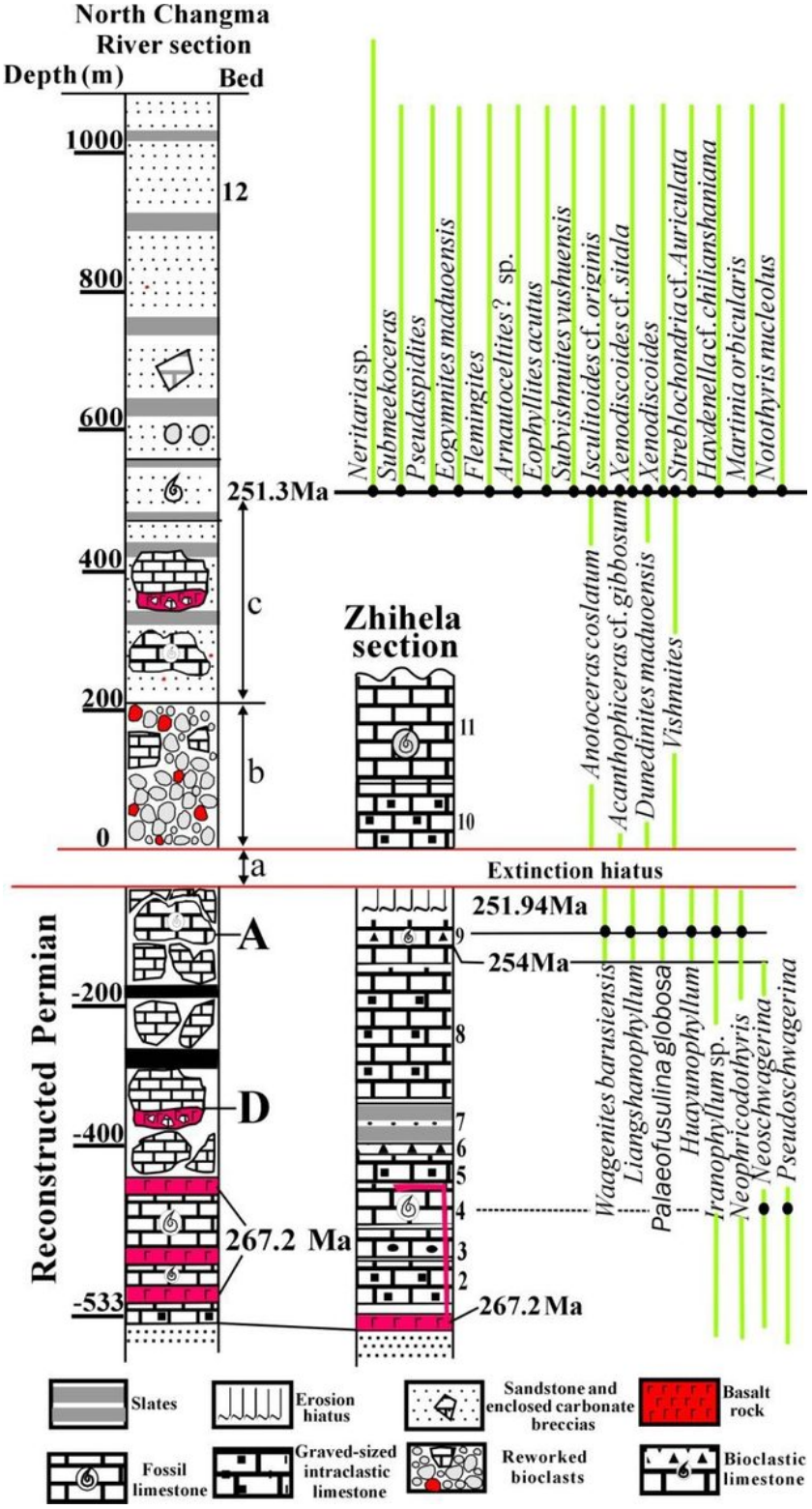

Figure 9

Correlation between the reconstructed Permian biostratigraphic sequence and the measured Zhihela across the PTB interval shows that a sea-level drop of 354 m led to erosion of the last 15-Myr Permian strata as thick as 533 m during the end-Permian regression. Numbered lines (a to c) represent a period of sea-level drop (extinction hiatus), sea-level low-stand, and sea-level rise or volcanic eruptions, respectively, as shown in Fig.1. A and D are magebreccias showing in Figure 5. A, D.

Supplementary Files

This is a list of supplementary files associated with this preprint. Click to download.

- carbonatedblocks.pdf
- sectiondata.pdf
- publishedfossilcollectionsinthestudyarea.pdf